On freshwater and the density-driven circulation in the northern seas

Erwin Lambert

Thesis for the degree of philosophiae doctor (PhD)
at the University of Bergen

2017

Date of defence: 29 November

Acknowledgements

I would like to start with thanking my three supervisors. Peter, thanks for all the (short-term) feedback on my writing despite your incredibly full agenda. Mike, thanks for all the discussions, guidance, and tips; and in particular for the warm welcome at WHOI. And most of all, Tor, thank you for introducing me to the world of science. I am sincerely grateful both for the freedom you've given me to find my own path, and for looking over my shoulder to prevent me from throwing myself in a ditch on the way.

The research leading to this dissertation has been funded by the Research Council of Norway project NORTH. Further travel support was granted by Resclim and Ocean Outlook.

Throughout these three years, I've met an incredible amount of smart, friendly, and enthusiastic people through Resclim, FAMOS, and ASOF, and during visits in Oslo and Stockholm. Being out with these communities, talking science in great environments, has been a major motivation for me to do science and to continue in academics. This also applies to the oceanography PhD's with whom I've had a great round of weekly discussion sessions. A big thanks goes out to Laura and Paul for giving me a chance to experience the real Arctic Ocean. But probably the best scientific experience of the last three years was through the annual PhD conference. Because honestly, what's better than networking with Scandianvian fellow-PhDs in the sauna on a remote island or in a little mountain hut?

To my co-authors Aleksi, Per and Mehmet, thank you for all the help, especially during those crisis-moments. This third paper would not have been here without any of you. And also thanks to Ingo and Mats for the technical help with NorESM. To Malin, Sara and Per, thanks for making Sweden a home. Camille, thank you for your office; this one smells great by the way! And to the last-minute-reading-team: Rike, Marius, Morven, Aleksi, and Lisbeth, you guys are great, cheers for reading through my thesis and papers on such short notice; especially the last two who've probably read this complete dissertation at least once.

I'd like to thank my officemates, and in particular my housemates Lander, Meike and Fran for all the fun and for dealing with my grumpy face during the last period; this period would have been a lot harder if you guys hadn't been around. And it would have been impossible without the weekly football and volleyball sessions making sure I could vent my head on a regular basis. It's been a lot of fun on the field! And although I've met a lot of really great people throughout these last three years, I would especially like to thank – in random order – Lander, Patrik, Nora, and Aleksi for all the good times.

Finally, to family and friends, thank you for allowing me to retreat into my little bubble. This dissertation would not have been here without your patience and your unconditional support.

Abstract

The Arctic Ocean and the Nordic Seas are freshening, in part due to anthropogenic climate change. Within the northern seas, seawater density is in part dominated by temperature, and in part by salinity. This reflects on the density-driven circulation in the northern seas which consists of two coupled branches of circulation: an overturning branch dominated by temperature, and an estuarine branch dominated by salinity. In order to assess how observed and projected increase in freshwater input into the northern seas can change this circulation, a better understanding of its governing dynamics is required.

Using a hierarchy of theory and models, this dissertation studies how freshwater impacts the strength, stability, and variability of the density-driven circulation in the northern seas. Whereas freshwater is commonly perceived as suppressing a temperature-dominated circulation, models of various complexity indicate that increased freshwater input into low-salinity surface waters can spin up the salinity-dominated circulation. This results in a freshwater-induced increase in the poleward transport of Atlantic Water and heat. The coupling of the two circulation branches stabilises the density-driven circulation with respect to perturbations in freshwater, and abrupt transitions in the temperature-dominated circulation can only be induced by sufficient, localized freshwater input into dense surface waters. Finally, the transient response of the temperature- and salinity-modification of Atlantic Water in the Arctic Ocean to perturbations in Arctic river runoff is quantified; this indicates a potential predictability of regional processes at monthly resolution.

This dissertation describes the unique behaviour of coupled temperature- and salinity-dominated branches of density-driven ocean circulation. It reveals a glimpse of the largely unexplored potential for interaction between subtropical and polar ocean circulation. For the northern seas, this interaction translates into freshwater-sensitivity of the density-driven circulation that appears relatively weak and less dominant than what is commonly understood. As this circulation is integrated in the large-scale ocean circulation beyond the northern seas, these findings would have implications for the sensitivity of the global ocean circulation to future perturbations in high-latitude freshwater input.

List of papers

I Lambert, E., T. Eldevik, and P. M. Haugan (2016). How northern freshwater input can stabilise thermohaline circulation, *Tellus A.*, **68**, 31051, doi:10.3402/tellusa.v68.31051

II Lambert, E., T. Eldevik, and M. A. Spall, On the dynamics and water mass transformation of a boundary current connecting alpha- and beta- oceans, *submitted to Journal of Physical Oceanography*

III Lambert, E., A. Nummelin, P. Pemberton, and M. Ilıcak, Tracing the imprint of river runoff variability on Arctic water mass transformation, *prepared for submission to Journal of Geophysical Research: Oceans*.

Contents

Chapter 1

Introduction

The origin of large-scale physical oceanography can be traced back to one bucket of water. In 1751, an English slave trading ship crossed the North Atlantic around 25°N (*Ellis*, 1751). Henry Ellis ordered the lowering of a bucket, with a thermometer in it, to different depths. The surface ocean was measured at 29°C, but as they lowered the bucket deeper, temperatures decreased down to 12°C at a depth of 1200 m. From these measurements, *Thompson* (1798) rightfully drew a number of conclusions. First, this cold deep water must have originated in the higher latitudes where similarly cold waters are found at the surface. Second, these cold waters must have been transported toward the deep ocean at lower latitudes. And third, this transport must have been compensated by a shallower transport from the low to high latitudes. Connecting these dots, the observations from Ellis could only be explained by a net large-scale ocean circulation. Today, this is referred to as the Atlantic meridional overturning circulation.

The above example shows how much insight can be gained from logical reasoning and simplification of a complex system. Because computational resources and observations have long been sparse, much of the early oceanographic work consisted of the development of theories based on limited observations. Today, a range of state-of-the-art coupled climate models are available and the pool of in-situ and remote observations is growing on a daily basis. However, theoretical oceanography remains a very valuable approach to gain an understanding of the fundamental processes that govern the ocean, and to define the ocean's role in the climate system.

> "It seems that if one is working from the point of view of getting beauty in one's equations, and if one has really a sound insight, one is on the sure line of progress. If there is not complete agreement between the results of one's work and experiment, one should not allow oneself to be too discouraged, because the discrepancy may well be due to minor features that are not properly taken into account and that will be cleared up with further development of the theory"
>
> *Paul Dirac*[1]

[1] Published in Scientific American, May 1963

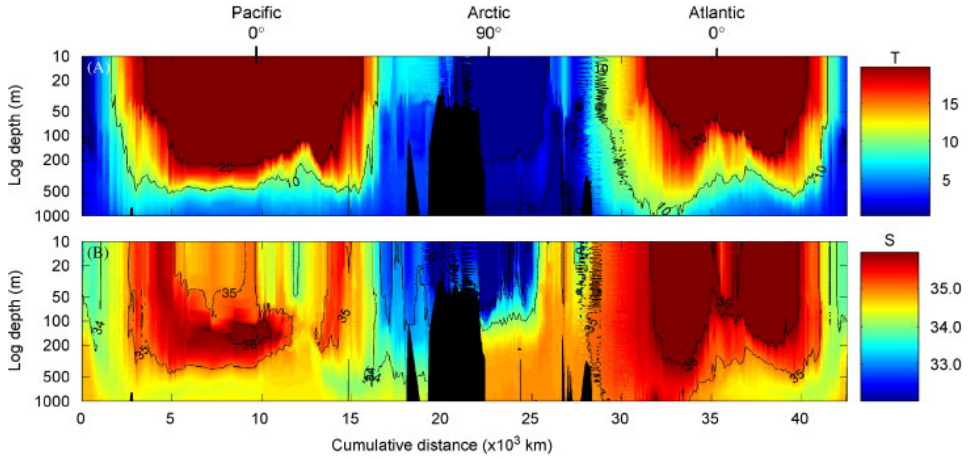

Figure 1.1: Global temperature and salinity distribution. Vertical and quasi-meridional sections from the Pacific sector of the Southern Ocean (left), across the Arctic (middle), to the Atlantic sector of the Southern Ocean (right). Upper panel: potential temperature in $^\circ C$, lower panel: salinity. In the (sub)tropics, vertical density gradients are dominated by temperature. In the polar regions, they are dominated by salinity. Data are from WOCE and JWACS, figure is from *Carmack* (2007).

The need for such fundamental understanding is becoming more and more pressing. As human activity alters the Earth's climate system, the ocean unravels its importance (*Solomon et al.*, 2007). In part, the ocean has functioned as a buffer in the climate's adjustment to enhanced atmospheric greenhouse gas concentrations. The upper 700m of the global ocean has absorbed 90% of the excess heat trapped in the climate system during the last 50 years (*Bindoff et al.*, 2007); and during the last 10 years, the deep ocean between 700 and 2000m has absorbed 30% of the global ocean heat uptake (*Balmaseda et al.*, 2013).

Although this oceanic heat uptake moderates atmospheric warming, it also induces a number of indirect effects of anthropogenic climate change. Warming of the upper ocean accelerates melt of Arctic sea ice (*Polyakov et al.*, 2010) and marine-terminating glaciers (*Straneo et al.*, 2013); warming of the upper and deep oceans contributes to global sea level rise (*Levitus et al.*, 2012); and oceanic warming, together with atmospheric warming, enhances the global hydrological cycle (*Helm et al.*, 2010). Each of these effects may perturb the global ocean circulation with potential consequences for the future adjustment of Earth's climate.

As measured by Henry Ellis' crew in 1751, warm waters in the subtropical North Atlantic reside on top of cold waters. This vertical temperature gradient is stable, as warm waters, through thermal expansion, have a lower density than cold waters. Two decades after these measurements, Captain Cook sailed on his second voyage to the Southern Ocean. At 55$^\circ S$, they measured sea surface temperatures at -1$^\circ C$; yet as they lowered a thermometer to 180 m depth, temperatures rose to +1$^\circ C$ (*Hakluyt Society*, 1961). As recognised by Captain Bellingshausen in 1819, cold waters can reside on top of warm waters because of an accompanying vertical salinity gradient (*Hakluyt Society*,

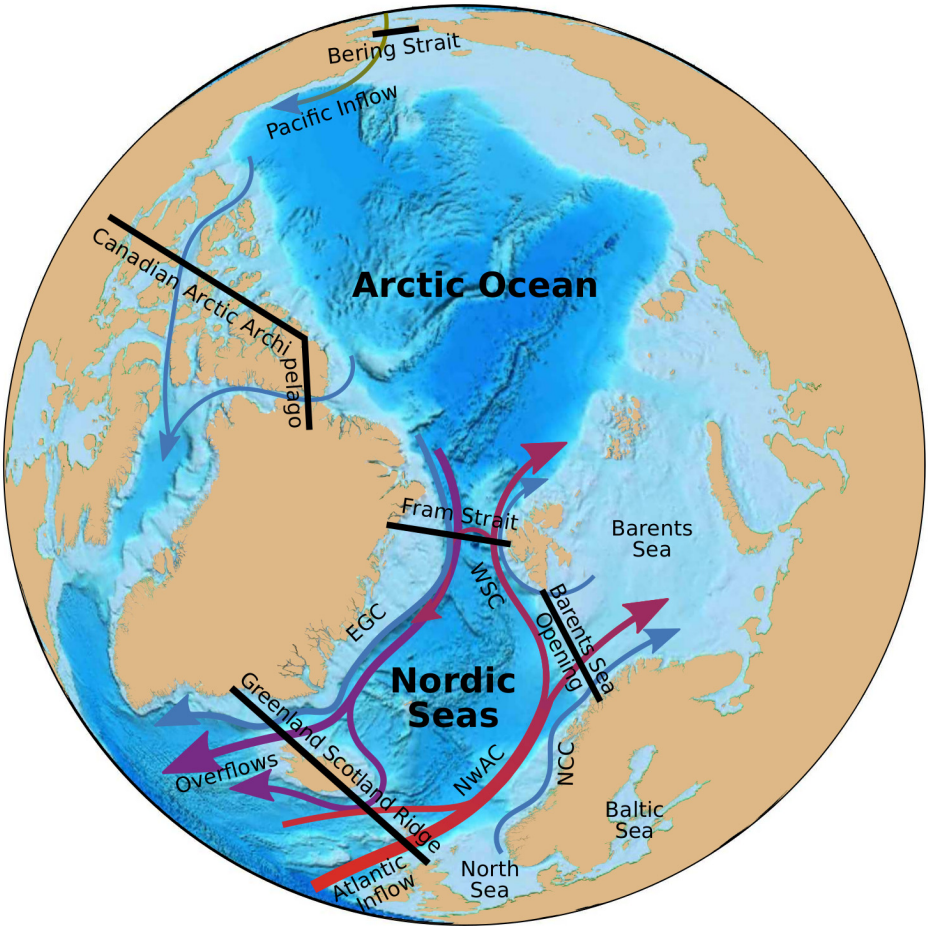

Figure 1.2: The northern seas, more commonly referred to as the Arctic Mediterranean. Arrows indicate schematic circulation patterns of the major water masses that cross the gateways: Atlantic Water (red), Deep Water (purple), Polar Water (blue), and Pacific Water (green). Abbreviated currents are NwAC: Norwegian Atlantic Current; NCC: Norwegian Coastal Current; WSC: West Spitsbergen Current; EGC: East Greenland Current. Shading of the oceanic regions represents topography; the large lightblue areas are the continental shelves, typically shallower than 500 meters.

1945; *Roden*, 1964). As surface waters in these high latitudes are relatively fresh, compared to the deeper, more saline waters, density still increases with depth. The qualitative difference between these observed temperature- and salinity-profiles allows for a distinction between oceanic regions that are temperature-dominated, and those that are salinity-dominated. As can be seen in Fig. 1.1, this distinction applies to most regions across the globe, and separates the temperature-dominated (sub)tropics from the salinity-dominated polar regions.

The cold deep water observed in the subtropical North Atlantic could only be explained by a large-scale circulation. Without this circulation, diffusion of heat would, over time, warm the deep ocean. Similarly, a large-scale circulation is required to maintain the relatively saline deep water in the higher latitudes. This circulation is the salinity-dominated counterpart of the overturning circulation. In analogy to regional circulation patterns in fjords and riverine outlets, this salinity-dominated circulation is called an estuarine circulation. The qualitative contrast between the temperature-dominated subtropics and the salinity-dominated polar regions thus reflects qualitatively opposing large-scale circulation patterns.

A convenient way to study large-scale circulation patterns is by focusing on mediterranean seas. These seas are almost entirely surrounded by land, with the exception of relatively narrow gateways which connect the seas to the global ocean. The typically clear definition of these gateways, which mark the boundaries of the mediterranean seas, facilitates the combined effort from theoretical, modeling, and observational studies. One example of such a mediterranean sea lies in the northern seas: the Arctic Mediterranean (*Sverdrup et al.*, 1942). This is a collective name for the Nordic Seas and the Arctic Ocean.

Due to its southern extent, the Arctic Mediterranean host regions where salinity dominates density, as well as regions where temperature dominates density. Moreover, one of the clearest signs of climate change is the observed increase in freshwater input into the Arctic Mediterranean (*Haine et al.*, 2015; *Serreze et al.*, 2006). This dissertation studies the impact of changes in freshwater input on the Arctic Mediterranean's density-driven circulation. In the coming section, I provide an overview of the temperature- and salinity-dominated density-driven circulation in the global ocean. This is followed by a more detailed description of the circulation patterns in the Arctic Mediterranean. Finally, I give an overview of freshwater in the Arctic Mediterranean and its potential impact on density-driven circulation.

Chapter 2

Background

2.1 Density-driven circulation

The large-scale circulation in the global ocean is commonly attributed to two ultimate driving forces: wind and buoyancy forcing (see, for example, *Gill* (1982)). Buoyancy forcing is the combined term for all surface fluxes that modify sea surface temperature and salinity, and hence sea surface density. Wind can drive ocean circulation by providing mechanical energy; whereas buoyancy forcing can drive circulation by providing potential energy (e.g., *Wunsch et al.*, 2004). This difference indicates two qualitative circulation patterns, although they are not independent.

It should be stated up front that this division between wind- and density-driven circulation is imperfect, as both driving forces limit each other's potential to drive circulation. Vertical density gradients limit the downward penetration of mechanical energy by wind; and similarly wind-induced mixing is required for the downward penetration of potential energy provided by buoyancy forcing. Despite the limitations, dividing between wind- and density-driven circulation is an old practice[1] that has provided a great amount of knowledge about ocean circulation.

2.1.1 Seawater density

The density of seawater relates to large-scale ocean circulation through thermal wind balance. This balance consists of a horizontal component, geostrophic balance, and a vertical component, hydrostatic balance. Thermal wind balance prescribes a first-order relation between horizontal density gradients and vertical velocity gradients. Due to rotational effects, meridional gradients in density are coupled to vertical gradients in zonal velocities, and vice versa. Thermal wind balance applies to large regions in the ocean interior, away from boundary layers near the ocean floor, the sea surface, and

[1] With regards to the relative impact of wind and buoyancy forcing on global ocean circulation, *Robinson and Stommel* (1959) noted: "The exchange of letters in NATURE during the 1870's between W. B. Carpenter and James Croll shows how futile simple verbal arguments can be in discussing such issues. The reader with a morbid interest in fallacious verbal theories may find it entertaining to look over the work of the English eccentric William Leighton Jordan, "The Ocean, its tides and currents and their causes", Longman's Green and Co., London, 1873."

continental margins. Understanding the large-scale density-driven circulation therefore requires an understanding of horizontal density gradients in the global ocean.

The density of seawater is determined by three components: pressure, temperature[2], and salinity. Pressure increases seawater through compression. This provides a background vertical gradient in ocean densities, yet it does not directly impact horizontal density gradients. The relation between density and temperature is determined by the thermal expansion coefficient α. In practically all cases relevant to the ocean, this coefficient is a negative number, indicating that higher temperatures decrease seawater density. The relation between density and salinity is determined by the haline contraction coefficient β. This value is always positive, indicating that higher salinities increase seawater density.

As the measurements during the 18th and early 19th centuries indicated, density in large regions throughout the global ocean are dominated by either temperature or salinity. In reference to the coefficients of thermal expansion and haline contraction, these regions are referred to as the alpha- and beta-oceans respectively (*Carmack*, 2007). Density in the alpha-oceans is dominated by temperature for two reasons. First, temperature gradients are relatively large compared to salinity gradients; and second, the thermal expansion coefficient α is relatively large in warm waters. In the beta-oceans, temperature gradients are relatively small, in part because seawater cannot cool below freezing point; and, whereas the haline contraction coefficient β is relatively constant in the ocean, the thermal expansion coefficient decreases with temperature and nearly vanishes in the polar regions. Along with the relatively large salinity gradients, this accounts for the salinity-dominance in the beta-oceans.

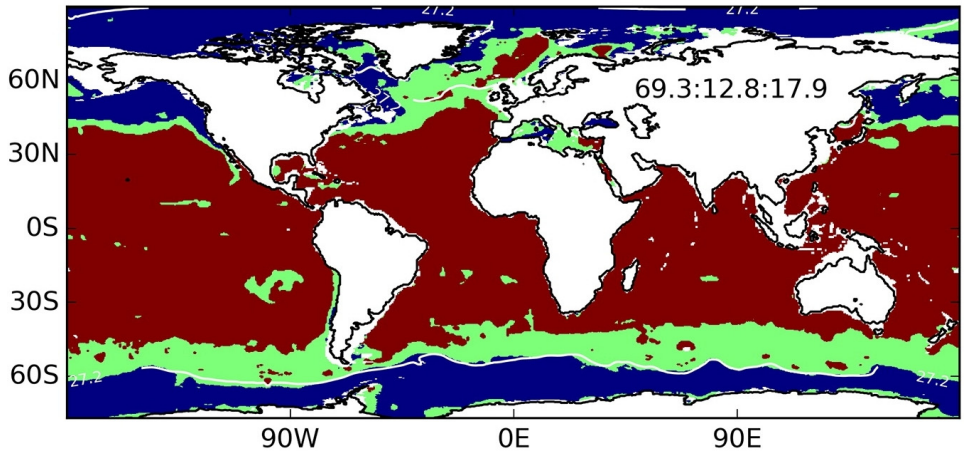

Figure 2.1: Transition zones at 100m. Red: the temperature-dominated alpha-oceans, blue: the salinity-dominated beta-oceans, Green: the transition zones. Numbers over the Eurasian continent quantify the fraction of the global ocean covered by these three regions at this specific depth. Figure from *Stewart and Haine* (2016).

[2]Through compression, temperatures increase with depth. Potential temperature denotes the temperature a water parcel would have when brought to the sea surface. This is usually denoted by Θ, but I will use T for simplicity.

The large-scale alpha- and beta-oceans converge in so-called transition zones (*Sverdrup et al.*, 1942). In these transition zones, density is alternately dominated by temperature or salinity (*Stewart and Haine*, 2016). As temperature and salinity gradients, as well as the thermal expansion coefficient, vary with depth the locations of the transition zones vary with depth as well. In the upper few hundred meters below the surface mixed layer, the transition zones largely overlap with the subpolar oceans (Fig. 2.1). These include the Southern Ocean, the North Pacific, the Labrador and Irminger Seas, and large regions in the Nordic Seas and the Barents Sea which are part of the Arctic Mediterranean.

2.1.2 The global thermohaline circulation

Much of our current understanding of density-driven circulation originates from the model presented by *Stommel* (1961). Stommel presented an idealized model for two connected basins, each filled with a different well-mixed water mass. This type of model is now referred to as a box-model. Stommel designed the model to describe a circulation that is driven by the density difference between the two water masses. As a result, cooling of one basin, and warming of the other, drives a temperature-dominated overturning circulation. Although Stommel did not apply this model explicitly to the ocean, its construction was motivated by the observation that oceanic temperatures and salinities have the tendency to covary.

This global covariance between temperature and salinity is a direct result of the global hydrological cycle. Warm waters in the (sub)tropics are subject to net evaporation, whereas cold waters in the (sub)polar regions receive net precipitation and river runoff. As a result, gradients in temperature and salinity tend to have opposite effects on density. Including a freshwater cycle in his model, Stommel showed that, with a sufficiently strong freshwater cycle, the box-model's circulation can reverse and become salinity-dominated. Such a salinity-dominated circulation is commonly referred to as an estuarine circulation. As the box-model can sustain density-driven circulation dominated by either temperature or salinity, Stommel called this a thermohaline circulation.

Throughout the global oceans, there are examples of both temperature-dominated overturning circulations and salinity-dominated estuarine circulations. The best known example is the Atlantic meridional overturning circulation (AMOC, e.g., *Kuhlbrodt et al.*, 2007). This is the circulation described by *Thompson* (1798), and is maintained by cooling and sinking in the subpolar North Atlantic (*Nansen*, 1912). Another overturning circulation exists in the Southern Ocean, which is maintained by cooling and sinking in the Weddell Sea (*Wüst*, 1939). There even exist indications that the Antarctic Circumpolar Current may be driven by meridional temperature-dominated density gradients (*Hogg*, 2010).

Besides these two large-scale overturning circulations, a number of large-scale circulation branches have been described as estuarine circulations. These include the circulation in the North Pacific (*Tully and Barber*, 1960), the circulation in the Arctic Ocean (*Stigebrandt*, 1981), and the exchange between the North Pacific and the Arctic Ocean across the Bering Strait (*Stigebrandt*, 1984); these estuarine circulations are all maintained by the relatively large freshwater fluxes into the North Pacific and the

Arctic Ocean. In addition, a variety of Stommel's box-model was presented by *Rooth* (1982) in which the AMOC is driven by the salinity-difference between the northern and southern high latitudes; and *Marotzke* (2000) suggests that due to its interhemispheric nature, AMOC dynamics may be better represented by Rooth's model than by Stommel's. Despite the lack of a clear definition, as discussed by *Wunsch* (2002), these branches of temperature- or salinity-dominated circulation are commonly referred to as the global thermohaline circulation.

Although Stommel's box-model provides useful insight into density-driven ocean circulation, it lacks two essential processes. The first is the gradual transformation of surface currents due to buoyancy forcing; the second is subsurface mixing of dense and light waters. These two processes are water mass transformations. A simplest expansion of the box-model to represent water mass transformation is the loop-model (*Huang*, 1999; *Welander*, 1967). Loop-models illustrate the relative importance between surface water mass transformation, allowing for waters to sink, and internal water mass transformation, necessary for waters to return to the surface (*Wunsch*, 2005). The importance for internal mixing was already noted by *Sandström* (1908) and has been actively discussed since (e.g., *Munk and Wunsch*, 1998; *Munk*, 1966; *Stommel*, 1958). This internal mixing is commonly attributed to wind and turbulence generated by breaking internal waves (e.g., *Nikurashin and Ferrari*, 2013; *Wunsch et al.*, 2004). Yet new evidence suggests that boundary layers near topography may play an important role (*Ferrari et al.*, 2016; *McDougall and Ferrari*, 2017).

The interplay between ocean circulation, surface buoyancy forcing, and internal (mixing) processes was described by *Walin* (1977, 1982). Rather than using geographical coordinates, Walin presented a framework for ocean circulation and water mass transformation in either temperature- or salinity-coordinates. This concept was expanded by *Speer* (1993) into a framework for ocean circulation in combined temperature-salinity space. Although the framework does not describe dynamics, it has proved a useful tool for understanding global and regional circulation. For example, this framework has led to the description of the global thermohaline circulation in terms of temperature- and salinity-modification rather than horizontal or vertical ocean currents (*Döös et al.*, 2012; *Zika et al.*, 2012). Using this framework, the relative contributions of surface buoyancy forcing and internal processes to global circulation have been isolated (*Groeskamp et al.*, 2014, 2017; *Hieronymus et al.*, 2014). Further, this framework has been applied to study the impact of freshwater input on ocean circulation in the Arctic Ocean (*Pemberton et al.*, 2015).

2.2 The Arctic Mediterranean

The Arctic Mediterranean (AM) connects to the global ocean through exchanges across its defining gateways: the Greenland Scotland Ridge, the Bering Strait, and the straits in the Canadian Arctic Archipelago[3] (Fig. 1.2). These exchanges can be summarized as three branches of the global thermohaline circulation.

[3] I will here ignore any exchanges across the English Channel.

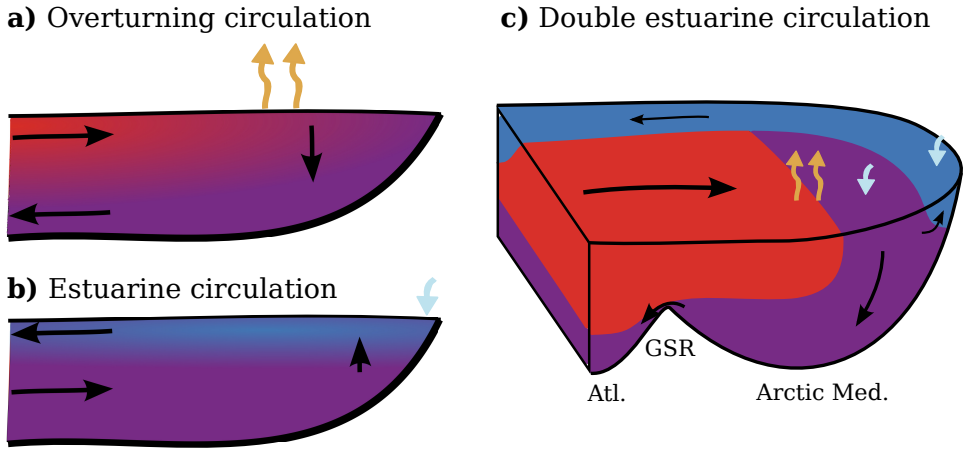

Figure 2.2: Illustration of density-driven circulation patterns in a marginal sea. a) An overturning circulation, dominated by temperature and governed by surface heat loss. b) An estuarine circulation, dominated by salinity and governed by freshwater input. c) A double estuarine circulation coupling subtropical and polar circulation patterns. This circulation pattern is observed in the Arctic Mediterranean and is related to the combined temperature- and salinity-dominance in the transition zone. Panel c is taken from **Paper I** (*Lambert et al.*, 2016).

The first branch is the exchange across the Bering Strait, and consists of a net inflow of Pacific Water (*Stigebrandt*, 1984). Due to its shallow and narrow extent, volume exchanges across the Bering Strait are relatively small (approx. 1 Sv, *Woodgate et al.*, 2012). Therefore, the role of the Pacific inflow in the AM is commonly reduced to its net transport of heat and freshwater. The major outflow pathway of Pacific Water is through the Canadian Arctic Archipelago (*Rudels and Friedrich*, 2000).

The other two branches of the global thermohaline circulation that flow through the AM constitute the circulation of ATlantic Water. These circulation branches are an overturning circulation (Fig. 2.2a) and an estuarine circulation (Fig. 2.2b), and reflect the extent of the alpha- and beta-oceans in the AM. A total of 8.5 Sv of Atlantic Water enters the AM across the Greenland Scotland Ridge (*Hansen et al.*, 2008; *Østerhus et al.*, 2005). Of this Atlantic inflow, approximately 2/3 parttakes in the overturning circulation; and the residual 1/3 in the estuarine circulation (*Hansen and Østerhus*, 2000). As the overturning and the estuarine circulations are coupled by a common inflow, this circulation type is defined as a double estuarine circulation (*Stigebrandt*, 1985, Fig. 2.2c). The return flow of the double estuarine circulation is predominantly across the Greenland Scotland Ridge, although a fraction of O(1 Sv) of the estuarine circulation exits through the Canadian Arctic Archipelago (*Beszczynska-Möller et al.*, 2011).

2.2.1 Overturning circulation

Early observations by *Nansen* (1912) indicated a dense outflow from the Arctic Mediterranean across Denmark Strait. Such dense waters feed the deep overturning branch of the AMOC (*Swift et al.*, 1980) and are estimated to account for 2/3 of the AMOC's deep equatorward branch (*Dickson and Brown*, 1994). It has long been thought that these dense waters are the direct product of deep convection (e.g., *Aagaard et al.*, 1985), as well as brine rejection during sea ice growth (e.g., *Midttun*, 1985). However, based on observations, *Mauritzen* (1996a,b) proposed a new circulation scheme for the overturning circulation in the AM. This scheme describes a downwelling cyclonic boundary current that gradually loses heat and increases in density.

Of the 8.5 Sv of Atlantic Water that enters the Arctic Mediterranean, a total of 6 Sv exits through the Denmark Strait and the Faroe Bank Channel (*Dickson et al.*, 2008). These in- and outflows are connected by a number of overturning loops. Two relatively short connections are observed in the Norwegian Sea (*Eldevik et al.*, 2009) and the Iceland basin (*Våge et al.*, 2013). A longer circulation, yet still confined to the Nordic Seas, is maintained by eddy-controlled recirculation in the Fram Strait (*Hattermann et al.*, 2016; *von Appen et al.*, 2016). Finally, two branches of Atlantic Water penetrate the Arctic Ocean through the Barents Sea Opening and Fram Strait (e.g., *Rudels*, 2016). The distribution of Atlantic Water between these two gateways is thought to be governed by local winds (*Furevik*, 1998; *Lien et al.*, 2013). Recently, *Mauritzen et al.* (2011) has mapped out these different overturning loops, connecting the Atlantic inflow to the dense overflows.

A dynamical description for a warm inflow into a marginal sea, subject to surface heat loss was given by *Visbeck et al.* (1996). They illustrated how surface heat loss from a basin interior can induce a baroclinic inflow that circulates a basin as a rim current. A similar description was given by *Spall* (2004) based on a topographically controlled boundary current. Both studies suggested that a lateral exchange of heat governed by baroclinic eddies could warm the interior sea surface and enhance the total heat loss. These eddies are primarily formed in regions of steep topography such as the eastern Nordic Seas (*Broomé and Nilsson*, 2016; *Isachsen*, 2011), which is one of the dominant regions of surface heat loss in the Arctic Mediterranean (*Isachsen et al.*, 2007), along with the Barents Sea (*Årthun et al.*, 2011).

The magnitude of the inflow feeding such an overturning circulation has been suggested to be set by thermal wind balance across the gateway. This implies that the Atlantic inflow would be a function of the temperature contrast between the inflowing waters and the interior (*Spall*, 2011) and the depth of the gateway (*Walin et al.*, 2004). As such an inflow cools downstream, *Straneo* (2006) indicated that a gradual transformation from a baroclinic to a more bartropic boundary current can explain the net downwelling in a marginal sea, associated with the overturning circulation.

2.2.2 Estuarine circulation

The estuarine circulation in the Arctic Mediterranean was first described by *Stigebrandt* (1981). This circulation is commonly attributed to processes in the Arctic Ocean. Two processes that can maintain an estuarine circulation were proposed by *Rudels* (1989). The first is by entrainment of Atlantic Water across the halocline, which is limited by the strong salinity-stratification. The second, which Rudels proposed to be the presently dominant process, is by exchange between river runoff and the Atlantic Water boundary current in the shelf regions. In addition, seasonal growth and melt of sea ice has been suggested as a formation process for Polar Water in the Barents Sea (*Steele et al.*, 1995) and north of Svalbard (e.g., *Rudels*, 2016).

Besides the Arctic Ocean, significant formation of low-salinity waters is observed in the margins of the Nordic Seas. Along the eastern boundary, the transport of low-salinity water by the Norwegian Coastal Current strengthens from 0.1 Sv at the Baltic opening (*Winsor et al.*, 2001) to 0.7 Sv at the Barents Sea opening (*Björk et al.*, 2001; *Blindheim*, 1989; *Skagseth et al.*, 2011). Also along the coast of West Spitsbergen, formation of low-salinity waters is observed (*Saloranta and Haugan*, 2004). And in the western boundary, Polar Water transport, carried southward by the East Greenland Current, increases downstream (*Håvik et al.*, 2017) from 1-1.5 Sv across the Fram Strait (*de Steur et al.*, 2014) to approximately 2 Sv across the Greenland Scotland Ridge (*de Steur et al.*, 2017; *Sutherland and Pickart*, 2008). These observations point to a significant contribution of processes in the Nordic Seas to the total Polar Water formation in the AM.

Throughout the AM, these observed low-salinity waters are transported by baroclinic coastal currents. A description for the transport of such a low-salinity boundary current was given by *Werenskiold* (1935) based on thermal wind balance. A balance between river runoff and exchange between a coastal current and offshore waters was proposed by *Whitney and Garvine* (2005) to be governed by wind-driven Ekman transport. A similar balance was suggested for the coastal current circulating the Arctic Ocean between river runoff and lateral salt fluxes governed by baroclinic eddies (*Spall*, 2013). In a conceptual model for the Hudson and James Bay, *St-Laurent et al.* (2012) showed that the observed circulation of a coastal current can be relatively well represented by a combination of both Ekman transport and eddy-exchange. In general though, knowledge of the dynamics of high-latitude coastal currents is limited by sparse observations, not in the least because many of them are covered by sea ice (*Bacon et al.*, 2008).

2.3 Freshwater

At the moment freshwater enters the ocean, it loses its clear identity by mixing with saline seawater. This complicates the quantification of freshwater in the ocean. The oceanic branch of the global hydrological cycle is therefore relatively ambiguous and is commonly identified by an equatorward transport of low salinity waters. The transport and storage of freshwater in the ocean is typically quantified with respect to a reference salinity, assuming these low salinity waters are a mixture of freshwater and seawater

of this reference salinity. For the Arctic Ocean, *Aagaard et al.* (1985) proposed a reference salinity of 34.8 which is the approximate mean salinity of water in the Arctic. For the Nordic Seas, *Dickson et al.* (2007) use a reference salinity of 35.2 which is the approximate mean salinity of Atlantic Inflow. Although both choices are valid in their own right, and consistent use reference salinities allows for intercomparison between studies of different disciplines, they remain approximations. As a result, measured freshwater fluxes from, i.e., runoff cannot be directly compared to oceanic freshwater transports (e.g., *Tsubouchi et al.*, 2012).

Freshwater can be temporarily extract from the ocean due to freezing of its surface waters. During sea ice formation in winter, salt remains behind in a comparable way to evaporation; this is called brine rejection. Although some salt is stored in sea ice, its salinity is typically on the order of 5-10% of the seawater below (e.g., *Maykut*, 1985). Hence, sea-ice is often interpreted as carrying freshwater which can be stored for the season, or for several years, before melt returns this freshwater to the ocean, reducing surface salinities in a comparable way to precipitation. Sea ice can be transported over significant distances before melting, because of wind and ocean currents. As this transport of sea ice is largely equatorward, it forms a branch of freshwater transport from the region of sea ice growth to the region of sea ice melt; and can therefore be interpreted as locally contributing to the oceanic return pathway of the global hydrological cycle.

The volume fluxes of freshwater are typically more than an order of magnitude smaller than ocean transports. For example, volume transport in and out of the Arctic Mediterranean are approximately 10 Sv (*Mauritzen et al.*, 2011), whereas total freshwater input into the Arctic Ocean is approximately 0.3 Sv (e.g., *Haine et al.*, 2015; *Serreze et al.*, 2006). The impact of freshwater on the volume budgets of ocean basins is therefore small. However, this is not the case for its impact on surface salinities. Freshwater fluxes are therefore often represented as virtual salt fluxes. This representation neglects perturbations in volume, but takes into account the impact on sea surface salinities.

2.3.1 Sources, pathways, and sinks

Freshwater fluxes are often expressed in terms of mSv rather than Sv, reflecting its relatively small volume flux compared to oceanic volume transports. A number of studies have attempted to quantify the freshwater input into the Arctic Ocean due to river runoff (*Peterson et al.*, 2002) or its total amount (*Serreze et al.*, 2006). The most recent of these freshwater budgets was presented by *Haine et al.* (2015) based on the period 2000–2010; estimating a total freshwater input of 300mSv. The dominant source of freshwater is runoff from the Eurasian and Canadian rivers (130 mSv, see Fig. 2.3), freshwater carried by the Pacific inflow across Bering Strait (80 mSv, relative to $S = 34.8$), net precipitation-evaporation (70 mSv), and Greenland melt (12 mSv). Additionally, the Nordic Seas receive approximately 60 mSv of freshwater from the outflow from the Baltic and the North Sea (20 mSv, *Winsor et al.*, 2001), net precipitation-evaporation (20 mSv), river runoff from the Norwegian coast (11 mSv) and Greenland melt (9 mSv, *Dickson et al.*, 2007).

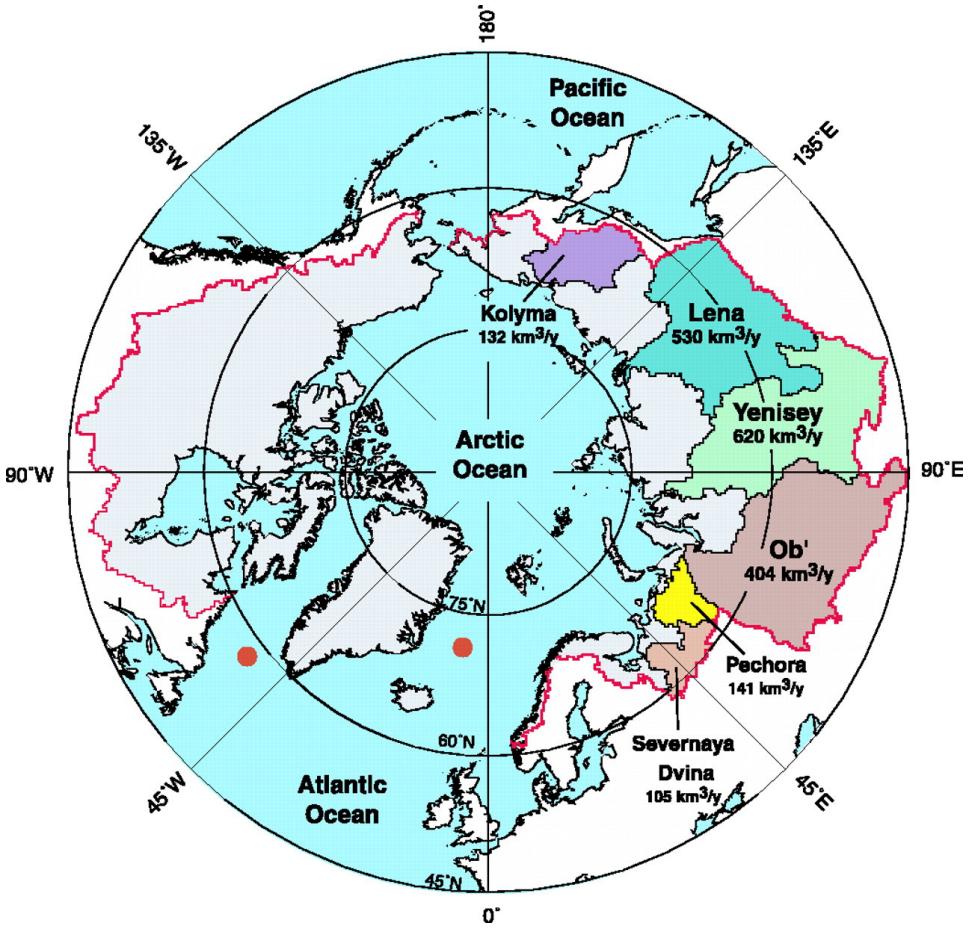

Figure 2.3: Catchment areas of river runoff to the Arctic Mediterranean. Numbers indicate freshwater fluxes from the individual rivers in km^3/yr. 1 mSv of freshwater is equivalent to 32 km^3/yr. Figure from *Peterson et al.* (2002).

The sinks of freshwater from the Arctic Mediterranean were estimated by *Dickson et al.* (2007) at 300 mSv (using a reference salinity of 35.2). Of this, approximately 150 mSv exits with Polar Water carried by the East Greenland Current across the Greenland Scotland Ridge, approximately 100 mSv exits across the straits in the Canadian Arctic Archipelago, and approximately 50 mSv is carried out by the dense overflow waters across Denmark Strait and the Faroe Bank Channel. In terms of the double estuarine circulation, this implies that, in total, 1/6 of the freshwater input into the Arctic Mediterranean exits with the overturning circulation.

It is insightful to try and attribute the sinks of freshwater, and in particular the freshwater outflow by the overturning circulation, to the different freshwater sources. The most likely source of freshwater carried out by the dense overflows is precipitation into the Nordic Seas (20 mSv) and the Barents Sea (an unknown amount), where dense water is formed at the surface. All other sources of freshwater enter low-salinity surface

waters. To account for a total 50 mSv of freshwater to be exported by the dense overflows, this implies that up to 30 mSv of freshwater from these other sources crosses the halocline that separates low-salinity waters from the dense overflows. This can be interpreted as freshwater leakage, and constitutes roughly 10% of the total freshwater input that enters low-salinity surface waters in the Arctic Mediterranean.

Freshwater input into the Arctic Mediterranean is increasing. The net freshwater inflow from the Pacific across the Bering Strait has increased by 30 mSv during the period 2001–2011 (*Woodgate et al.*, 2012). Similarly, river runoff and net precipitation-evaporation into the Arctic Ocean have increased by 10 and 15 mSv respectively from the period 1980–2000 to the period 2000–2010 (*Haine et al.*, 2015). Finally, the freshwater flux due to Greenland melt has increased as well, though by a small amount of approximately 1-2 mSv during the period 1992–2010 (*Bamber et al.*, 2012). These increases in freshwater input necessarily affect the freshwater storage and/or the freshwater export of the Arctic Mediterranean.

Over the period 1992–2012, liquid freshwater storage in the Arctic Ocean has increased with an average rate of approximately 20 mSv (*Rabe et al.*, 2014). In part, this enhanced liquid freshwater storage results from decreased freshwater storage in sea ice (*McPhee et al.*, 2009). Much of the excess freshwater in the Arctic Mediterranean is stored in the Beaufort gyre, as indicated by *Proshutinsky et al.* (2009). The gyre's potential for freshwater storage is strongly coupled to atmospheric variability, in particular the Arctic Oscillation (*Giles et al.*, 2012; *Serreze and Barrett*, 2011). The total freshwater input into the Arctic Ocean is projected to increase further during the next century due to enhanced net precipitation and river runoff (*Holland et al.*, 2007; *Vavrus et al.*, 2012). In addition, increased Greenland melt may start to play a significant role to changes in total freshwater input into the Arctic Mediterranean (*Little et al.*, 2016).

2.3.2 Potential impact on circulation

To understand the potential impact of freshwater input on an overturning circulation, we revisit the box-model of *Stommel* (1961). This model exhibits a salt-advection feedback that can induce a nonlinear response to increased freshwater input into the cold water. As a result, the model contains a threshold for freshwater input, beyond which a temperature-dominated overturning circulation cannot be maintained. Such behaviour has been reproduced in early global numerical models (*Bryan*, 1986; *Manabe and Stouffer*, 1988) and has raised concern about a potential future collapse of the AMOC (e.g., *Broecker*, 1997). Using so-called hosing experiments, where large freshwater fluxes are introduced to a model ocean, *Rahmstorf et al.* (2005) quantified the freshwater thresholds in a number of general circulation models.

Future Greenland melt is commonly seen as a potential candidate for similarly large freshwater perturbations. However, models forced with projected Greenland melt produce a relatively moderate weakening of the AMOC (*Jungclaus et al.*, 2006; *Lenaerts et al.*, 2015; *Weijer et al.*, 2012). *Weijer et al.* (2012) conclude that the equilibrium response does not depend on eddies; and *Lenaerts et al.* (2015) suggest that oceanic warming might have a larger effect on future weakening of the AMOC than increased freshwater input from Greenland melt. In addition, *Weijer et al.* (2012) indicate that

Greenland melt might have a small effect on the surface salinity of the Nordic Seas, compared to the Labrador Sea. Based on similar results, *Jungclaus et al.* (2006) conclude that the overflows across the Greenland Scotland Ridge are the 'backbone' of the AMOC, based on their stability.

Although an overturning circulation is commonly interpreted as being inhibited by freshwater input, this may be dependent on internal mixing. Following the arguments from *Sandström* (1908), *Nilsson and Walin* (2001) conclude that, if mixing is the limiting factor for an overturning circulation, increased freshwater input could even increase the overturning circulation. In contrast, when upwelling is not a limiting factor, stratification-dependent mixing can increase the freshwater-sensitivity of an overturning circulation (*Marzeion et al.*, 2007). As vertical mixing in global circulation models is commonly constant, *Marzeion and Levermann* (2009) conclude that freshwater-sensitivity of modeled AMOC may be underestimated. Additionally, the recent indications of significant mixing near topographic boundaries (*Ferrari et al.*, 2016; *McDougall and Ferrari*, 2017) may imply a different freshwater-sensitivity of the AMOC.

The freshwater input into the Arctic Mediterranean is an essential ingredient for sustaining the estuarine circulation. The impact of changes in freshwater input, however, are not so straightforward. *Nummelin et al.* (2015) show how increased river runoff in a column model for the Arctic Ocean increases salinity-stratification. As this stratification forms a barrier for mixing, *Nilsson and Walin* (2010) indicated that this increased stratification may either strengthen or weaken the estuarine circulation, dependent on mixing. Perturbing Arctic river runoff in a global ocean model, *Nummelin et al.* (2016) report a slight increase in total volume exchange across the Arctic gateways for relatively small increases below 30%; and a decrease for larger perturbations. Similar experiments were performed by *Pemberton and Nilsson* (2016) who find relatively insensitive volume exchanges to increased runoff.

Despite the observed increased freshwater input into the Arctic Mediterranean, no significant trends are as of yet observed in the Atlantic overturning circulation (*Haine*, 2016). And *Olsen et al.* (2008) report that overflows across the Greenland Scotland Ridge, both observed and modeled, are relatively stable. Is this a sign of the ocean's inertia, and is it merely a matter of time before we will observe freshwater-induced changes in ocean circulation? Or is there an inherent insensitivity of the density-driven circulation in the Arctic Mediterranean to freshwater perturbations? Little is known about the freshwater-sensitivity of a double estuarine circulation as observed in the Arctic Mediterranean. Based on a diagnostic model, *Eldevik and Nilsen* (2013) conclude that freshwater input may affect the relative strength of the overturning and estuarine circulation more strongly than the total inflow. However, this model does not describe any dynamics governing the circulation. Increasing the understanding of these dynamics is one of the primary goals of this dissertation.

Chapter 3

Motivation and objectives

The Arctic Mediterranean are freshening as a result of anthropogenic climate change. The theoretical work by *Stommel* (1961) and *Rooth* (1982) has induced concern that increased high-latitude freshwater input my strongly alter the global thermohaline circulation due to weakening, or even a collapse, of the AMOC. Across the Greenland Scotland Ridge, two branches of the global thermohaline circulation circulate the Arctic Mediterranean. These branches form a double estuarine circulation: a coupled system of a temperature-dominated overturning circulation and a salinity-dominated estuarine circulation.

If we wish to anticipate how increased freshwater input into the Arctic Mediterranean may affect ocean circulation, both temperature- and salinity-dominated barnches of the global thermohaline circulation must be accounted for. This dissertation sets two goals. First, it aims to contribute to the current understanding of the freshwater impact on the density-driven circulation in the Arctic Mediterranean. Second, it aims to illustrate unique dynamics associated with the transition zones between the subtropics and the polar regions. To achieve these two goals, this dissertation addresses three primary questions related to the freshwater impact on coupled temperature- and salinity-dominated ocean circulation. A gradual increase in model complexity allows for the development of a deep understanding of the underlying processes, and for the placement of these processes in a wider context. The three central questions addressed in this dissertation are:

I **How can freshwater input affect the stability of circulation?**

The box-model of *Stommel* (1961) postulates that a temperature-dominated overturning circulation can be reversed through changes in freshwater input. In **Paper I**, we extend this model to a minimal representation of a double estuarine circulation as observed in the Arctic Mediterranean. Using this extended box-model, we apply linear stability analysis to quantify the freshwater input required to destabilize the embedded overturning circulation. A comparison to Stommel's stability analysis allows for a direct quantification of the changed stability due to the coupling of the overturning and the estuarine circulations.

II **How can spatial variation in runoff affect water mass transformation and circulation?**

The overturning circulation in the Arctic Mediterranean has been described by *Mauritzen* (1996a) as a downstream densifying boundary current that circulates the basin. A number of conceptual studies have reasonably reproduced such an overturning boundary current based on surface heat loss (e.g., *Spall*, 2004; *Straneo*, 2006; *Walin et al.*, 2004). In **Paper II**, we postulate that the estuarine circulation in the Arctic Mediterranean can, in part, be similarly described by freshening of the boundary current. By constructing a boundary current model for a double estuarine circulation, we study the impact of freshwater input that enters the shelf regions surrounding the basin. Motivated by the observed freshwater sources of the Nordic Seas, we demonstrate the importance of spatial variation in freshwater input by representing of the Baltic and Arctic outflows and comparing their relative impact on the circulation.

III **How can temporal variation in runoff affect water mass transformation?**

The first two papers regard steady-state circulations and **Paper II** discusses explicit geographical distribution of freshwater input. As noted by *Haine et al.* (2015), river runoff is the freshwater source for the Arctic Ocean that exhibits the largest seasonal to interannual variability. In **Paper III**, we extend our exploration of coupled temperature- and salinity-dominated circulation to trace the impact of temporally varying river runoff on water mass transformation in the Arctic Ocean. Simultaneously, we increase the model complexity, with respect to the first two papers, by using a global coupled ocean-sea ice model (NorESM2, *Bentsen et al.*, 2013). This global model allows for quantification of the relative effect of runoff variability to other processes bypassed in the first two papers, primarily the seasonal cycle of ice growth and melt.

Chapter 4

Summary of papers

Paper I: *How northern freshwater input can stabilise thermohaline circulation*

In **Paper I**, we extend the box-model of *Stommel* (1961) to study the impact of freshwater input on the stability of a double estuarine circulation. This extended model consists of three boxes which represent the three qualitative water masses observed in the Arctic Mediterranean: Atlantic Water, Deep Water[1] and Polar Water. The overturning circulation is driven by the temperature-dominated density contrast between Atlantic and Deep Water; whereas the estuarine circulation is driven by the salinity-dominated density contrast between Deep and Polar Water.

As in Stommel's model, changes in freshwater input can induce qualitative transitions leading to a reversal of the overturning branch. This reversal is marked by a switch to a salinity-dominated density contrast between Atlantic and Deep Water. However, the coupled estuarine circulation greatly stabilises the overturning circulation, requiring stronger freshwater input to induce a transition than in absence of this estuarine circulation. Particularly, we find that the impact of freshwater input is more dependent on its distribution – whether it feeds into fresh Polar Water or dense Deep Water – than its total amount.

The model construction allows for a stable circulation regime which we call the throughflow state. In this regime, the overturning circulation is reversed, but the estuarine circulation dominates total volume transport. As a result, this circulation regime allows for an Atlantic inflow along the surface without dense water formation.

Paper II: *On the dynamics and water mass transformation of a boundary current connecting alpha- and beta- oceans*

In **Paper II**, we formulate a model for a double estuarine circulation as a boundary current circulating a marginal sea such as the Nordic Seas. This model takes the concept from **Paper I** and introduces topography, parametrized water mass transformation, and thermal wind balance. The model is forced with freshwater input into the shelf regions,

[1] In **Paper I**, we refer to this water mass as Overflow Water; but in the more general context of this dissertation, I choose to systematically refer to this water mass as Deep Water.

representing the dominant freshwater sources of the Nordic Seas. In contrast to interior precipitation, freshwater input into the shelf regions has a slight strengthening effect on the Atlantic inflow.

The dominant impact of freshwater input is its effect on the outflow strength of Polar and Deep Water, in agreement with the box-model presented in **Paper I**. This freshwater impact is determined not only by the actual freshwater flux, but also strongly by the location where it enters the shelf regions. For the Nordic Seas, this implies that perturbations in the Baltic outflow, an important freshwater source which enters near the Atlantic inflow, may have an order of magnitude larger potential to impact exchanges across the Greenland Scotland Ridge than perturbations in the Arctic outflow. This illustrates explicitly the connection between water mass transformation in the alpha- and beta- oceans.

In addition to **Paper II**, I present a set of idealized numerical simulations with a primitive equation model (MITgcm, *Marshall et al.*, 1997). This model is configured to resemble the boundary current model in **Paper II**. The model's freshwater forcing is divided between precipitation into the interior and runoff onto the shelves; this division is equivalent to the freshwater forcing of the box-model in **Paper I**. The numerical simulations align with results from both conceptual models, as increased runoff spins up both the estuarine circulation and the Atlantic inflow. This response differs qualitatively from the response to interior precipitation, which weakens the Atlantic inflow and induces an abrupt transition similar to *Spall* (2012).

Paper III: *Tracing the imprint of river runoff variability on Arctic water mass transformation*

In **Paper III**, we further increase the complexity of the system by using a global coupled ocean-sea ice model (NorESM2, *Bentsen et al.*, 2013). Although the model is run at coarse resolution, hence not resolving eddies, the use of a global model introduces a large number processes which are not included in **Papers I** and **II** such as realistic wind fields, growth and melt of sea ice, and seasonality. Diagnosing water mass transformation in terms of salinity- and temperature-transformation illustrates the model's representation of an estuarine and an overturning circulation in the Arctic Ocean. Increasing Arctic river runoff by 30% induces an increase in both heat and salt import into the Arctic Ocean. This enhanced heat import, which induces enhanced surface heat loss, is a response to increased salt diffusion, implying an estuarine response in the modeled Arctic Ocean.

The transient response of Arctic water mass transformation to runoff perturbations reveals a wide range of timescales from several months up to 5 years. These response timescales can be attributed to delayed propagation of runoff-induced anomalies due to the shelf break, depth, and the freshwater export by the circulations of Atlantic and Pacific Water. In order to quantify the predictive skill of runoff, we introduce a novel tool which we call the seasonal Climate Response Function. This method allows for potential prediction of regional water mass transformation at monthly resolution and performs well in predicting modeled salinity-transformation based on variability in total Arctic river runoff.

Chapter 5

Perspectives

5.1 General conclusions

The results from the three papers combined provide an illustration of the interaction between a salinity-dominated branch of density-driven circulation and a temperature-dominated one. As freshwater input has an inherently opposite effect on both circulation branches, the total freshwater-sensitivity of the coupled density-driven circulation is weaker than that of its separate components.

The conceptual models in **Papers I** and **II** illustrate how freshwater input can spin up an estuarine circulation, and consequently strengthen the inflow of Atlantic Water. This response is reproduced in an idealized numerical model, presented in Sec. 6.2.1. A similar response is found in the general circulation model presented in **Paper III**, where increased Arctic runoff induces an enhanced heat transport into the Arctic Ocean. This strengthening of circulation is induced when freshwater predominantly enters relatively fresh surface waters, and is in contrast to the more commonly addressed impact of freshwater input into dense surface waters such as the interior of the Nordic Seas.

The coupling of an overturning and an estuarine circulation also alters the stability of the density-driven circulation with respect to freshwater perturbations. Possible instability of density-driven circulation is governed by the salt-advection feedback of *Stommel* (1961). As illustrated in **Paper I**, enhanced salt advection, due to a freshwater-induced spinup of the estuarine circulation, stabilises the overturning circulation. Similar to the box-model, runoff into low-salinity shelf waters cannot induce an abrupt transition in the numerical simulations presented in Sec. 6.2.1. Because only moderate runoff perturbations were applied in **Paper III**, in order to prevent a non-linear response, no salt-advection feedback could be detected in the general circulation model experiments.

To complement these steady-state responses to freshwater perturbations, **Paper III** addresses the transient response to runoff. The results in this paper allow for tracing the imprint of runoff variability throughout the Arctic Ocean, and illustrate the potential predictability of water mass transformation based on high-latitude freshwater input.

5.2 Open questions and recommendations

The inevitable result of science is that it always raises more questions than it answers. Here, I provide a number of open questions, raised by the study leading to this dissertation, that I consider worthy of further research. In addition, I provide recommendations on how these questions can be addressed.

Because this research focuses on the regional domain of the Arctic Mediterranean, processes that complete the circulation in the global ocean have not been studied. For both overturning and estuarine circulations, this completion depends on mixing of heat and salt in the global ocean, which may have an important effect on the response of the circulation to freshwater perturbations (e.g., *Munk*, 1966; *Stommel*, 1958). One way to study the impact of mixing on the freshwater-sensitivity of a double estuarine circulation is by designing a loop model for two coupled branches.

One of the essential ingredients for the freshwater-sensitivity of the density-driven circulation is found to be the surface salinity where freshwater enters the basin. In both models presented in **Papers I** and **II**, all freshwater that enters low-salinity surface waters was carried out by the estuarine circulation. However, as discussed in Sec. 2.3.1, roughly 10% of the freshwater input that enters low-salinity surface waters in the Arctic Mediterranean leaks across the halocline and flows out through the overturning circulation. In the box-model in **Paper I**, freshwater leakage can be implemented by a prescribed diffusion between the basins filled with Polar Water and Overflow Water, equivalent to how *Longworth et al.* (2005) represent a gyre circulation in a two-box model. In the boundary current model in **Paper II**, freshwater leakage can be implemented by reformulating the relation between cross-halocline diffusion and the transformation of Atlantic Water to Polar Water.

In **Paper I**, we conclude that the freshwater threshold, at which a temperature-dominated overturning circulation reverses, is dependent on the strength of the coupled estuarine circulation. This effect is not tested in the numerical model presented in Sec. 6.2.1, although this can be done relatively straightforwardly by reproducing the precipitation-experiment for different constant values of runoff.

The double estuarine circulation in the box-model in **Paper I** allows for a qualitatively new circulation state that cannot be attained by the two-box model by *Stommel* (1961); this is called the throughflow state (Fig. 5.1c,f). It was not addressed in this paper to what extent this circulation state can be realised in the real ocean. Palaeo-records from the Last Glacial Maximum suggest that the circulation in the Arctic Mediterranean during that period was qualitatively different from today (*Dokken and Jansen*, 1999; *Eldevik et al.*, 2014). These records can shed light into whether the circulation in the Arctic Mediterranean may once have resided in the throughflow state.

The simulations presented in **Paper III** show a significant impact of seasonal ice growth and melt on Arctic water mass transformation. As indicated by *Haine and Martin* (2017), this seasonal cycle is becoming more pronounced due to the rapid retreat of the summer sea ice edge. Additionally, river runoff into the Arctic Mediterranean is strongly concentrated in the summer months, and with a projected increase in runoff, this may further perturb the seasonal cycle. Temporal variability in freshwater input has

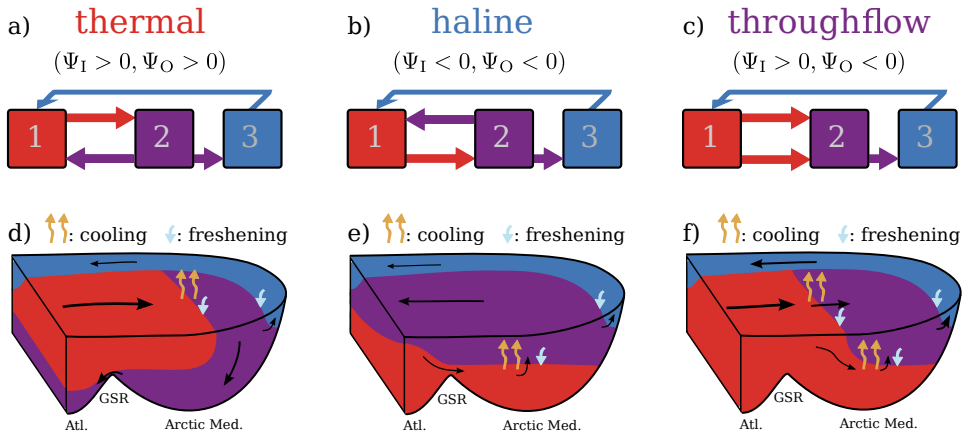

Figure 5.1: Three qualitative circulation patterns of a double estuarine circulation. Panels a,d represent the present-day circulation in the Arctic Mediterranean. Panels b,e represent a reversed overturning circulation similar to the haline circulation of *Stommel* (1961). Panels c,f represent an intermediate circulation pattern, called the throughflow state. The throughflow state is attained when the estuarine circulation is stronger than the reversed overturning circulation, and maintains a poleward heat transport. Figure from **Paper I** (*Lambert et al.*, 2016).

previously been applied in a box-model (*Cessi*, 1994) and in a boundary current model (*St-Laurent et al.*, 2012). These studies can form a basis for the inclusion of seasonal freshwater input into the models presented in **Papers I** and **II**.

A crucial reason for the existence of transition zones and beta-oceans is the nonlinear equation of state. Within the Arctic Mediterranean, the thermal expansion coefficient varies by an order of magnitude. This allows for the cabbeling effect, which plays a role in transition zone dynamics (*Nycander et al.*, 2015; *Stewart et al.*, 2017). In both models in **Papers I** and **II**, the nonlinear equation of state was accounted for by neglecting the temperature-contribution to the density contrast between Polar Water and surrounding waters. In particular in the boundary current model, variation in the thermal expansion coefficient may impact dynamics greatly. This could be included analytically using the nonlinear equation of state introduced by *Roquet et al.* (2015).

5.3 A wider perspective

I would like to end this section with two more personal views on climate research. First, as computational resources become more abundant and will soon allow for 'eddy-resolving' global coupled simulations, the present dissertation illustrates the concurrent need for theoretical work and process studies. Gradual improvement of global circulation models has induced a growing confidence in their applicability to the real climate system. Yet although they are undeniably useful tools, and I consider them the most designated tools for guiding policy, there is a clear danger of overconfidence. Global models will be dependent on parametrizations for decades to come, if not centuries. And these parametrizations can only be developed and improved on the basis of mea-

surements and physical understanding. I therefore advocate a continued focus on education and research of theoretical oceanography and climate physics.

Second, research develops over time; and one could argue that, during the last decades, climate research has evolved with immense speed compared to other fields. Two reasons for this are the social impact of its advancement, and the need for a scientific basis to the public debate on the anthropogenic influence of climate change. Unfortunately this need is still pressing today. Two turning points have particularly accelerated climate research. First, the introduction of global numerical models have greatly advanced our understanding despite their aforementioned limitations. Second, the establishment of the Intergovernmental Panel on Climate Change (IPCC) has greatly benefited climate research, and its intercommunication, by outlining the current state of affairs. If I can foresee a next turning point which researchers can actively facilitate, it is a significant shift away from discipline-based research. Although interdisciplarity has become a hot word in climate science, it often functions as a buzzword to aid in securing funding for disciplinary-based research. A great majority of climate processes are governed at the interfaces between the ocean, the atmosphere, the cryosphere, the biosphere, and all other relevant spheres. Still, the bulk of research – admittedly including this dissertation – interprets these components as being uncoupled. I view this shift away from discipline-based climate research as one of the major challenges for my scientific generation which can mark the next turning point in advancing our collective understanding of the climate system.

Chapter 6

Scientific results

I

Paper I

6.1 The impact of freshwater input on circulation stability

Lambert, E., T. Eldevik, and P. M. Haugan (2016), How northern freshwater input can stabilise thermohaline circulation, *Tellus A*, **68**, 31051, doi:10.3402/tellusa.v68.31051

Tellus SERIES A DYNAMIC METEOROLOGY AND OCEANOGRAPHY
PUBLISHED BY THE INTERNATIONAL METEOROLOGICAL INSTITUTE IN STOCKHOLM

How northern freshwater input can stabilise thermohaline circulation

By ERWIN LAMBERT[1,2]*, TOR ELDEVIK[1,2] and PETER M. HAUGAN[1,2], [1]*Geophysical Institute, University of Bergen, Bergen, Norway*; [2]*Bjerknes Centre for Climate Research, Bergen, Norway*

(Manuscript received 11 February 2016; in final form 14 October 2016)

ABSTRACT

The North Atlantic thermohaline circulation (THC) carries heat and salt towards the Arctic. This circulation is partly sustained by buoyancy loss and is generally believed to be inhibited by northern freshwater input as indicated by the 'box-model' of Stommel (1961). The inferred freshwater-sensitivity of the THC, however, varies considerably between studies, both quantitatively and qualitatively. The northernmost branch of the Atlantic THC, which forms a double estuarine circulation in the Arctic Mediterranean, is one example where both buoyancy loss and buoyancy gain facilitate circulation. We have built on Stommel's original concept to examine the freshwater-sensitivity of a double estuarine circulation. The net inflow into the double estuary is found to be more sensitive to a change in the distribution of freshwater than to a change in the total freshwater input. A double estuarine circulation is more stable than a single overturning, requiring a larger amount and more localised freshwater input into regions of buoyancy loss to induce a thermohaline 'collapse'. For the Arctic Mediterranean, these findings imply that the Atlantic inflow may be relatively insensitive to increased freshwater input. Complementing Stommel's thermal and haline flow regimes, the double estuarine circulation allows for a third: the *throughflow* regime. In this regime, a THC with warm poleward surface flow can be sustained without production of dense water; a decrease in high-latitude dense water formation does therefore not necessarily affect regional surface conditions as strongly as generally thought.

Keywords: Box-model, Arctic Mediterranean, freshwater-sensitivity, thermohaline circulation

1. Introduction

The Atlantic thermohaline circulation (THC) redistributes vast amounts of heat and salt (e.g. Kuhlbrodt et al., 2007). Heating of the ocean at low latitudes and cooling at high latitudes prescribes a poleward heat transport which is partly sustained by deep water formation in the North Atlantic Ocean and Nordic Seas, and upwelling in the south. The meridional gradient in surface heat fluxes induces a freshwater cycle with net evaporation from the warm waters and net precipitation and river runoff into the cold waters. This northern freshwater input is generally believed to inhibit the Atlantic THC as indicated by the box-model of Stommel (1961). We will argue, using an extension of this model, that this is not necessarily the case.

Stommel's box-model illustrates the influence of freshwater input on THC. The model consists of two well-mixed basins of water, one warm and one cold, which are connected along the surface and bottom to allow for an overturning circulation. The hydrostatic pressure difference at the bottom forces the deep cold water into the warm basin and induces a circulation; to compensate, warm water flows into the cold basin along the surface. In Section 2.3, we discuss to what extent this model can be projected on large-scale ocean circulation. Freshwater input into the model's cold basin inhibits this circulation and, when strong enough, induces a positive feedback between the volume transport and salt advection which leads to a reversal of the circulation. Hence, Stommel's model exhibits two stable circulation regimes.

Despite its idealised nature, or perhaps because of it, Stommel's model has provided much insight into the behaviour of THC. Although Stommel himself called it a 'toy-model' for the flow between two interconnected reservoirs, many analogies have been made with the Atlantic Meridional Overturning Circulation (AMOC). Bryan (1986) was the first to simulate multiple stable regimes of a THC in an ocean general circulation model (GCM), and Manabe and Stouffer (1988) found two stable regimes in a coupled ocean-atmosphere GCM. The analogy between Stommel's box-model and the Atlantic THC was further considered by Rahmstorf et al. (2005) who used the model to diagnose

*Corresponding author.
email: erwin.lambert@uib.no

Citation: Tellus A 2016, **68**, 31051, http://dx.doi.org/10.3402/tellusa.v68.31051

an AMOC 'collapse' in intermediate complexity GCMs in so-called freshwater hosing experiments. Such a collapse is often paralleled to a transition to a haline circulation regime, that is, a reversal. Recent GCM studies on the response of the AMOC to increased northern freshwater input over the 21st century, however, project a gradual weakening rather than a reversal, shutdown or even an abrupt reduction (Weaver et al., 2012).

The effect of salt advection on THC, as described by Stommel, is a direct result of the tendency of temperature to equilibrate faster than salt due to direct heat loss to the atmosphere. Another implication of this asymmetry between temperature and salinity is that combined heat loss and freshwater input can lead to initial buoyancy loss and subsequent buoyancy gain (Wåhlin et al., 2009). It is generally known that buoyancy gain can facilitate THC as well as buoyancy loss. In riverine outlets, freshwater input induces estuarine circulations due to entrainment of relatively saline surrounding water. Stigebrandt (1981) showed that also the upper circulation in the Arctic Ocean can be described as an estuarine circulation and it is the northern freshwater input that sustains this branch of THC. If we are to assess the influence of freshwater input on THC in general, it appears one needs to take into account both processes of buoyancy loss and buoyancy gain.

One example where both processes of buoyancy loss and buoyancy gain affect the circulation is the northernmost branch of the Atlantic THC. The Arctic Mediterranean forms an approximate semi-enclosed basin with the Greenland-Scotland Ridge (GSR) as its main gateway. The basin is subject to both heat loss and freshwater input which transforms an inflow of Atlantic water in two stages. First heat loss and freshwater input combine to induce net buoyancy loss, predominantly in the Nordic Seas and Barents Sea. Part of the produced dense water returns towards the Atlantic as overflow water (Isachsen et al., 2007): an overturning branch. The residual of the densified inflow is subject to net freshening and consequent buoyancy gain in the Arctic and eventually exits the Arctic Mediterranean as cold, fresh polar water through the East Greenland Current (Rudels, 1989): an estuarine branch. The combination of these overturning and estuarine branches comprises a double estuarine circulation (Stigebrandt, 1985; Rudels, 2010). Extending the classical model of Knudsen (1900) to a double estuary for the Arctic Mediterranean, Eldevik and Nilsen (2013) concluded that the present Atlantic inflow is more sensitive to changes in heat than freshwater fluxes.

Several authors have expanded Stommel's box-model to allow for more features of THC (Rooth, 1982; Welander, 1986; Thual and Mcwilliams, 1992; Rahmstorf, 1996). We will here construct a box-model which allows for THC associated with subsequent buoyancy loss and buoyancy gain. We do not aim for a fully realistic description of double estuarine circulation with all its processes and energetics. Rather, we aim to contrast the stability and freshwater-sensitivity of a double estuarine circulation to a single overturning circulation in an equivalent framework. In Section 2, we present two separate models for an overturning (Stommel, 1961) and an estuarine circulation (equivalent to Rooth, 1982); in Section 3, we construct a model for the double estuary and describe its qualitative behaviour. As a quantitative example, we will in Section 4 project the model onto the Arctic Mediterranean. Using this model, we show that a double estuarine circulation is more stable than a single overturning circulation. We further illustrate how a shutdown of dense water formation does not necessarily alter surface conditions qualitatively.

2. Overturning and estuarine circulation

Double estuarine circulation is the circulation of volume, heat and salt induced by two stages of watermass transformation due to surface buoyancy fluxes. A double estuary is the semi-enclosed basin in which the watermass transformation occurs. We will construct a minimal box-model for a double estuary subject to net heat loss and freshwater input which is in contact with an external reservoir of relatively warm, saline water (Fig. 1c). The three basins represent well-mixed reservoirs of the three associated watermasses, connected to allow two branches of circulation: an overturning and an estuarine branch.

For the construction of his two-box model, Stommel (1961) argued that heat diffuses faster than salt. We will expand on this idea by allowing for watermass transformation to occur in two stages. In the first stage, both cooling and freshening occur on different time scales; in addition, a second stage allows for freshening without further cooling. This distinction allows for an inflow to initially lose buoyancy during the first stage and gain buoyancy during the second. Outflow of water produced in the first stage (basin 2) completes an overturning branch, whereas outflow of water produced in the second stage (basin 3) completes an estuarine branch.

In this section, we decompose the model into two separate circulations by allowing either of these outflows (Fig. 1a and b). These separated circulations are defined as an overturning and an estuarine circulation, respectively. The review of these models is in line with the overview of Marotzke (2000) and generally uses his nomenclature and dimensionalisations. We aim to understand how equilibrium volume transports and their stability depend on the freshwater input into the (double) estuary. For this, we apply linear stability analysis, described in Appendix A and identify different bifurcations (e.g. Kuznetsov, 2013) that characterise the qualitative stability of circulation.

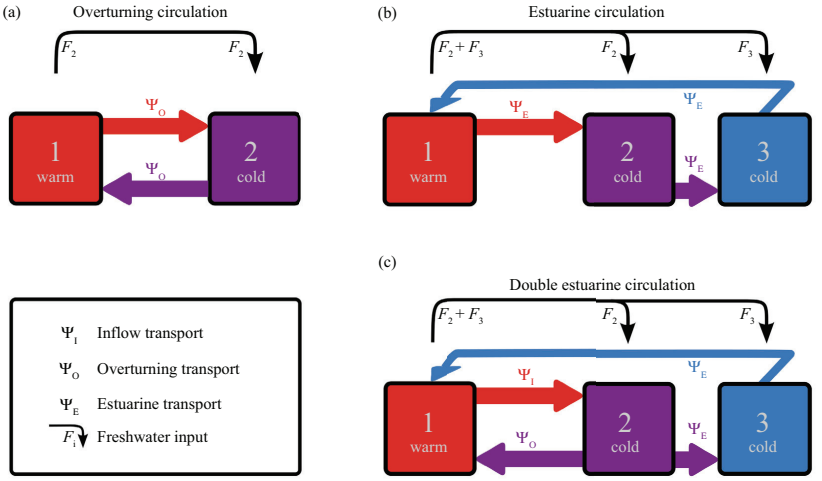

Fig. 1. Three-box model configurations. (a) Overturning (negative estuarine) circulation with volume transport Ψ_O, identical to the configuration of Stommel (1961), (Section 2.1); F_2 indicates the freshwater input into basin 2. (b) Estuarine circulation with volume transport Ψ_E, identical to the configuration of Rooth (1982), (Section 2.2). F_2 and F_3 indicate the freshwater input into the double estuary (basins 2 and 3). (c) Double estuarine circulation combining an overturning and estuarine branch (Section 3). The inflow transport Ψ_I into the double estuary is the sum of the overturning and estuarine transports. Arrows depict positive transports by convention.

2.1. Overturning circulation: Stommel (1961)

Overturning circulation only allows for outflow of the watermass produced in the first stage of transformation: cooling and freshening. For this circulation (Fig. 1a), we adopt Stommel's (1961) original box-model. This model consists of two well-mixed basins of water, connected by tubes of negligible volume. Conservation of salt in each of the basins can be written as

$$V_1 \frac{dS_1}{dt} = -|\Psi_O|\Delta S_{12} + F_2, \tag{1}$$

$$V_2 \frac{dS_2}{dt} = |\Psi_O|\Delta S_{12} - F_2, \tag{2}$$

where V_i is the volume of each basin; Ψ_O is the volume transport of the overturning, defined positive with surface flow from basin 1 to basin 2 (cf. Fig. 1a); $\Delta S_{ij} \equiv S_i - S_j$ is the salinity contrast between two basins; and F_2 is the freshwater input into basin 2, parametrised as a virtual salinity flux. An equal freshwater flux out of basin 1 closes the total freshwater budget. We will constrain F_2 to positive values.

Stommel closed the set of equations by assuming a linear relation between the volume transport and the hydrostatic pressure difference at the bottom of the basins. In order to contrast the double estuarine circulation to this well-established model for an overturning circulation, we generally assume the same linear relation introduced by Stommel. Further assuming a linear equation of state, we get a relation between the volume transport and the contrast in temperature and salinity between the basins:

$$\Psi_O = k_O \frac{\rho_2 - \rho_1}{\rho_{ref}} = k_O(\alpha\Delta T - \beta\Delta S_{12}), \tag{3}$$

where ρ_i is the density in each basin; ρ_{ref} is a reference density; α and β are the thermal and haline expansion coefficients; ΔT is the temperature difference between the warm basin 1 and the cold basins 2 and 3; and k_O is a hydraulic constant, relating the overturning transport to the density contrast induced by the watermass transformation.

We assume temperatures to be constant, with $\Delta T > 0$. This assumption is equivalent to applying a restoring condition for temperature with immediate relaxation to an ambient value (Marotzke, 2000).

We non-dimensionalise the system by introducing:

$$\tau = \frac{k_O \alpha \Delta T}{V_2} t, \tag{4}$$

$$f_i = \frac{\beta}{k_O \alpha^2 \Delta T^2} F_i, \tag{5}$$

$$s_{ij} = \frac{\beta}{\alpha \Delta T} \Delta S_{ij}, \tag{6}$$

which implies a scaling for the volume transport:

$$\Psi = \frac{1}{k_O \alpha \Delta T}\Psi. \tag{7}$$

This scaling applies to all volume transports throughout this study. Inserting eq. (3) into eq. (1) and (2) gives a single non-dimensional dynamical equation for the salinity contrast between the basins:

$$\frac{ds_{12}}{d\tau} = (1+\frac{V_2}{V_1})(-|1-s_{12}|s_{12}+f_2), \tag{8}$$

where the non-dimensional volume transport is:

$$\Psi_O = 1 - s_{12}. \tag{9}$$

The equilibrium solutions, denoted throughout the paper with an asterisk *, of eq. (8) are:

$$s_{12}^* = \begin{cases} \frac{1}{2} \pm \sqrt{\frac{1}{4}-f_2} & \text{if } s_{12} \le 1, \\ \frac{1}{2} + \sqrt{\frac{1}{4}+f_2} & \text{if } s_{12} > 1. \end{cases} \tag{10}$$

Note that these solutions are independent of the basin volumes. This is generally the case for all models presented in this study.

Combining eqns. (9) and (10) gives an equilibrium overturning transport Ψ_O^* as a function of the freshwater input into basin 2 (Fig. 2a). Each of the solutions in eq. (10) applies to a separate circulation regime. The first applies to the thermal regime (red curves in Fig. 2a), in which the surface transport is directed from basin 1 to basin 2 (cf. Fig. 1a). The negative root is stable and the positive root is unstable (cf. Appendix A.1). The second solution in eq. (10) applies to the haline regime (blue curve) in which the overturning is reversed with respect to the thermal regime.

Both stable thermal and haline equilibria are valid for a limited range of f_2. The thresholds that limit these equilibria are characterised by saddle-node bifurcations as indicated by the X's in Fig. 2a and are given by

$$f_2^X|_{th} = \frac{1}{4}, \tag{11}$$

$$f_2^X|_{ha} = 0, \tag{12}$$

where subscripts $|_{th}$ and $|_{ha}$ refer to the thermal and haline equilibria, respectively. Between these thresholds, a *bistability* region exists wherein both equilibria have a stable solution for the same amount of freshwater input.

The saddle-node bifurcations are a reflection of the salt-advection feedback in the system. Suppose that the system resides in its thermal equilibrium and $f_2 = 0$. A slow increase in f_2 will induce a salinity contrast and weaken the transport. Advection of salt by the inflow into basin 2 sustains the overturning circulation in its thermal regime. For values of $f_2 > f_2^X|_{th}$, the weakening of the transport suppresses the salt advection sufficiently for the system to enter a positive feedback loop which deems the thermal equilibrium unstable. This leads to an abrupt transition to the haline regime, wherein the circulation is reversed ($\Psi_O < 0$). To retrieve a thermal circulation, f_2 must be decreased below $f_2^X|_{ha}$, where the haline equilibrium is invalid. Note that this would require negative f_2 implying net evaporation from basin 2.

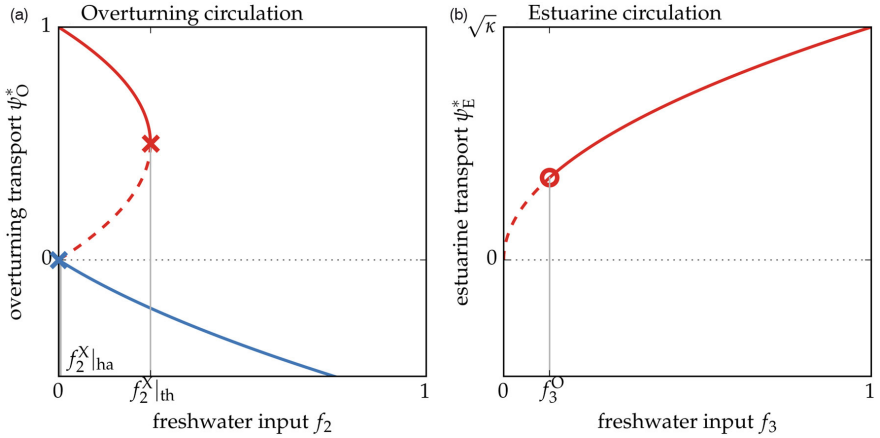

Fig. 2. Bifurcation diagrams for Stommel and Rooth's models. (a) Equilibrium overturning transport as a function of freshwater input into basin 2. Red and blue curves indicate thermal and haline regimes, respectively. X's indicate saddle-node bifurcations [cf. eqns. (11) and (12)]. (b) Equilibrium estuarine transport as a function of freshwater input into basin 3. O indicates a Hopf bifurcation [cf. eqns. (22)]. In both panels, solid (dashed) lines indicate stable (unstable) equilibria.

Stommel's model thus illustrates how a thermally driven overturning circulation can be inhibited by freshwater input, and can reverse to a stable haline circulation when a certain threshold is crossed. In a double estuary, however, this is only one effect of freshwater input, since the second circulation branch is an estuarine branch, facilitated by freshwater input.

2.2. Estuarine circulation: Rooth (1982)

Equivalently to the overturning, we can extract the estuarine branch from the double estuarine circulation by allowing only outflow of the watermass produced in the second stage of watermass transformation (Fig. 1b). This model for an estuarine circulation consists of three basins, representing the three watermasses involved in the circulation. Warm, saline water from basin 1 is cooled and freshened as it flows into basin 2. Rather than a direct return flow as in the overturning circulation, this water undergoes subsequent freshening (buoyancy gain) as it flows into basin 3. The cold and fresh water from basin 3 then constitutes the outflow from the double estuary into basin 1. Closer inspection of this model reveals that the configuration is identical to the box-model of Rooth (1982), in his case representing a more global version of Stommel's model with one equatorial and two high-latitude basins. We will however restrict the application of this model to an estuarine circulation.

The second stage of watermass transformation induces a density difference between basins 2 and 3. We assume a linear relation between this density difference and the estuarine transport, equivalent to eq. (3). Further using the same formulation of salt conservation as for the overturning, we write the model equations as:

$$V_1 \frac{dS_1}{dt} = -\Psi_E(\Delta S_{12} + \Delta S_{23}) + F_2 + F_3, \tag{13}$$

$$V_2 \frac{dS_2}{dt} = \Psi_E \Delta S_{12} - F_2, \tag{14}$$

$$V_3 \frac{dS_3}{dt} = \Psi_E \Delta S_{23} - F_3, \tag{15}$$

with volume transport Ψ_E:

$$\Psi_E = k_E \frac{\rho_2 - \rho_3}{\rho_{ref}} = k_E \beta \Delta S_{23}. \tag{16}$$

Here, k_E is the hydraulic constant for the estuarine circulation. Two parameters now describe the freshwater forcing of the estuarine circulation. In eqns. (13–15), F_2 represents the freshwater input during the first stage of watermass transformation, also associated with heat loss. F_3 represents the subsequent freshwater input after all heat from the warm inflow is lost. These same parameters, F_2 and F_3, will force the double estuarine circulation presented in the next section.

It should be noted that eqns. (13–15) apply only to a counter-clockwise estuarine circulation (cf. Fig. 1b). Because the model is symmetrical, equations for the clockwise circulation can be found by simply interchanging basins 2 and 3. As we will show in the next section, a counter-clockwise circulation of the estuarine branch can always be sustained with positive freshwater input into basin 3 ($F_3 > 0$) and we will therefore only consider $\Psi_E > 0$.

By combining eqns. (13–15) and (16), and scaling the system according to eqns. (4–7), we derive:

$$\frac{ds_{12}}{d\tau} = -(1 + \frac{V_2}{V_1})\kappa s_{12} s_{23} - \frac{V_2}{V_1}\kappa s_{23}^2 + (1 + \frac{V_2}{V_1}) f_2 + \frac{V_2}{V_1} f_3 \tag{17}$$

$$\frac{ds_{23}}{d\tau} = \kappa s_{12} s_{23} - \frac{V_2}{V_3}\kappa s_{23}^2 + \frac{V_2}{V_3} f_3 - f_2. \tag{18}$$

Here, $\kappa \equiv \frac{k_E}{k_O}$ is a non-dimensional parameter that sets the linear scaling of the estuarine circulation to density contrasts relative to that of the overturning circulation. For the estuarine circulation described in this section, this parameter is redundant, but it will become important for the double estuarine circulation. The non-dimensional volume transport of the estuarine circulation is:

$$\Psi_E = \kappa s_{23}. \tag{19}$$

The equilibrium solutions for eqns. (17) and (18) are:

$$s_{12}^* = \frac{f_2}{\sqrt{\kappa f_3}}, \tag{20}$$

$$s_{23}^* = \sqrt{\frac{f_3}{\kappa}}. \tag{21}$$

The equilibrium transport Ψ_E^* is only dependent on the freshwater input into basin 3 (Scott et al., 1999). This relation can be recognised directly by inserting eq. (16) into eq. (15).

Although the equilibrium transport is independent on f_2, this freshwater input does constrain the stability of the equilibrium. As shown in Appendix A.2, a Hopf bifurcation (O in Fig. 2b) appears when f_3 drops below a certain value, dependent on f_2. Since Hopf bifurcations are dependent on the transient response to a perturbation, and model timescales depend on basin volumes [eq. (4)], the location of the bifurcation is also dependent on the size of the basins:

$$f_3^O = \frac{f_2}{1 + V_2/V_1 + 2V_2/V_3}. \tag{22}$$

This value divides the equilibrium solution into a stable and an unstable region (Fig. 2b). For sufficient freshwater input into basin 3 ($f_3 > f_3^O$), the estuarine circulation is stable, increases with f_3 and is independent on f_2. For $f_3 < f_3^O$, the positive circulation is unstable and the assumed positive estuarine circulation ($\Psi_E > 0$) cannot be sustained.

This instability is related to a positive feedback associated with the salt advection from basin 1 into basin 2 as discussed by Scott et al. (1999).

2.3. On model assumptions

The models for an overturning and estuarine circulation described above are essentially two configurations of the same model. Both configurations, as well as other varieties derived from Stommel's original concept, are by construction idealisations. This makes them analytically tractable and conceptually appealing. When constructing our double estuary model in Section 3, we will retain the model physics of Stommel (and Rooth). We can accordingly benefit from existing understanding and established concepts of THC (e.g. the salt-advection feedback) associated with these models, but we are at the same time adopting the assumptions and caveats of the model physics.

The main assumptions at the heart of the models presented in this study include: 1) constant temperatures; 2) a closed freshwater cycle; 3) well-mixed basins; and 4) volume transports scaling linearly with density differences between basins. The latter constitutes the model's dynamical closure that completes the mathematical formulation at the level of salt conservation. The schematic of 'boxes and pipes' (e.g. Fig. 1) is thus a visualisation of the salt budget and not concerned with the details of ocean circulation and ocean basins beyond salt conservation.

Temperature is generally understood to equilibrate faster than salinity. In the case of constant temperatures (equivalent to Marotzke, 2000), this equilibration takes place instantaneously compared to the time scale of the changing salt budget. In our specific application to the Arctic Mediterranean (Section 4), this time scale is equal to 40 yr when considering the typical temperature contrast between the North Atlantic and the Arctic Ocean (about 10 K, see Table 1). The simplest relaxation is to a constant temperature contrast. Although this is generally unrealistic, we may expect variations in temperature contrast between low and high latitudes on these temporal and spatial scales to be on the order of degrees, moderate compared to its mean.

In order to construct any model for THC which allows for non-transient equilibria, one requires a closed freshwater cycle or relaxation of salinity. The models presented here assume a closed freshwater cycle, where net evaporation instantaneously balances net freshwater input. This assumption appears less applicable in a regional setting, because salt is only conserved on a global scale. However, the sensitivity of salinity of each individual basin to the applied freshwater fluxes scales with the basin volumes. One can, for example, consider the limit of an arbitrarily large evaporating basin. In this limit, the evaporating basin retains a constant salinity and resembles a sponge layer, commonly applied in regional numerical simulations with GCMs. Freshwater parameters can then be interpreted as pure parameters of freshwater input. It is important to note here that equilibrium solutions of these models are generally independent on the choice of basin volumes.

Table 1. Model parameters

Parameter	Symbol	Value
Present state observations		
Salinity contrast Atlantic inflow and overflows	ΔS_{12}	0.3 psu
Salinity contrast overflows and polar water	ΔS_{23}	0.9 psu
Temperature contrast Atlantic inflow and outflows	ΔT	8 K
Volume transport Atlantic inflow	Ψ_{I}	8.5 Sv
Volume transport overflows	Ψ_{O}	6 Sv
Parameters		
Thermal expansion coefficient	α	10^{-4} K^{-1}
Haline contraction coefficient	β	8×10^{-4} psu^{-1}
Hydraulic constant overturning branch	k_{O}	10^4 Sv
Hydraulic constant estuarine branch	k_{E}	3×10^3 Sv
Volume basin 2	V_2	10^{16} m^3
Scaling terms		
Time	t	40 yr
Freshwater input (relative to 35 psu)	F_i	230 mSv
Salinity contrast	ΔS_{ij}	1 psu
Volume transport	Ψ	8 Sv

Thermohaline contrasts are from Eldevik and Nilsen (2013); volume transports from Hansen and Østerhus (2000).

The assumption of well-mixed basins invites for interpretation of these basins as reservoirs of certain water masses, by definition relatively homogeneous, rather than ocean basins. Advection of volume and salt between basins then requires transport through isopycnals dividing the associated water masses. By retaining volume in each basin, in other words restricting movement of these isopycnals, the models imply diapycnal mixing which is unspecified and excessive (e.g. Nilsson and Walin, 2001).

Also the assumption of linear scaling of volume transport with density differences is associated with excessive mixing. Guan and Huang (2008) showed that accounting for limited mixing energy can be expressed in a non-linear scaling in Stommel's model. This scaling reduces the sensitivity of circulation to changes in surface buoyancy fluxes, which should be taken into account when interpreting the quantitative analysis in Section 4.

The linear scaling of volume transport with density difference as introduced by Stommel has been a common and valid critique when applying the model to large-scale THC. The relation cannot be straightforwardly deduced from first principles (Marotzke, 2000). The simulated AMOC of many GCMs do however scale linearly with

the meridional density or hydrostatic pressure gradient (e.g. Griesel and Maqueda, 2006). Whether this consistency also reflects causality is admittedly a matter of much debate (Toggweiler and Samuels, 1995; Kuhlbrodt et al., 2007; de Boer et al., 2010).

In the case of the estuarine circulation, and particularly that associated with the Arctic, a linear scaling has been proposed by Werenskiold (1935). This argument, later adopted by Rudels (2010), is based on thermal wind balance between a fresh western boundary current (the outflow of the estuarine circulation) and relatively saline surrounding water. To what extent this holds and, more generally, how large-scale (Arctic) estuarine circulation is forced are also matters of debate (e.g. Rudels, 2012).

3. Double estuary model

The double estuarine circulation (Fig. 1c) allows for outflow of both watermasses produced during the first (basin 2) and second (basin 3) stages of transformation. The total circulation thus constitutes two branches: an overturning and estuarine branch. These two branches connect through the surface flow between basin 1 and 2 which is the inflow into the double estuary, defined as Ψ_I.

3.1. Model configuration

The volume transports of the separate branches, Ψ_O and Ψ_E, scale to density differences as in Stommel's and Rooth's models [eqns. (3) and (16)]. Conservation of volume implies:

$$\Psi_I = \Psi_O + \Psi_E. \tag{23}$$

Scaled according to eq. (7), this can be written as:

$$\Psi_I = \Psi_O + \Psi_E = 1 - s_{12} + \kappa s_{23}. \tag{24}$$

Here, we see that κ introduces a relative weight of the two stages of watermass transformation.

As discussed in Section 2.2, we will only consider $\Psi_E = \kappa s_{23} > 0$. Equation (24) then reveals three possible circulation regimes for the double estuarine circulation: the *thermal, haline* and *throughflow* regimes (Fig. 3a–c). The first two are qualitatively equivalent to the thermal and haline regimes of Stommel's overturning. The throughflow does not contain an overturning, neither thermal nor haline; rather, a flow is directed from basin 1 to basin 2 both at the surface and at depth.

The equations for conservation of salt, applying to all three circulation regimes, can be written as:

$$V_1 \frac{dS_1}{dt} = -\frac{1}{2}(\Psi_E + |\Psi_O| + |\Psi_I|)\Delta S_{12} - \Psi_E \Delta S_{23} + F_2 + F_3, \tag{25}$$

$$V_2 \frac{dS_2}{dt} = \frac{1}{2}(\Psi_E + |\Psi_O| + |\Psi_I|)\Delta S_{12} - F_2, \tag{26}$$

$$V_3 \frac{dS_3}{dt} = \Psi_E \Delta S_{23} - F_3. \tag{27}$$

This is a generalisation of the equations for each separate regime, given explicitly in Appendix B. In terms of non-

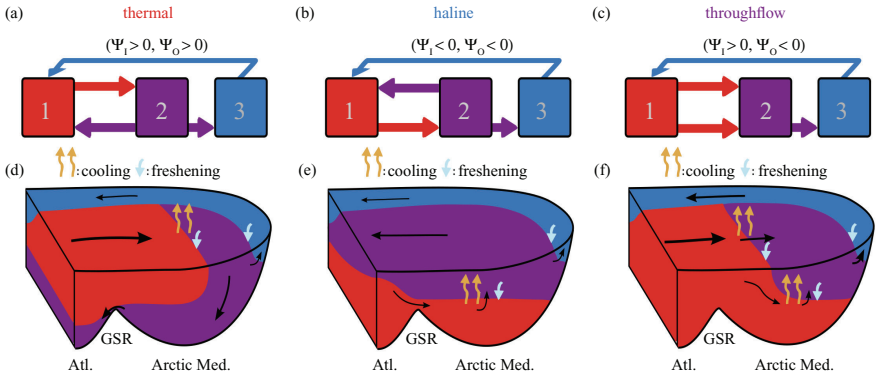

Fig. 3. Three flow regimes of the double estuary. (a–c) Qualitative flow directions which define the different regimes. (d–f) An interpretation of the corresponding regimes in an Arctic Mediterranean setting. The present state of the Arctic Mediterranean can be characterised as a thermal circulation (panel d).

dimensional salinity contrasts, combining eqns. (24) and (25–27), we derive:

$$\frac{ds_{12}}{d\tau} = -\frac{1}{2}(1+\frac{V_2}{V_1})(\kappa s_{23} + |1-s_{12}| + |1+\kappa s_{23} - s_{12}|)s_{12} - \frac{V_2}{V_1}\kappa s_{23}^2 + (1+\frac{V_2}{V_1})f_2 + \frac{V_2}{V_3}f_3, \tag{28}$$

$$\frac{ds_{23}}{d\tau} = \frac{1}{2}(\kappa s_{23} + |1-s_{12}| + |1+\kappa s_{23} - s_{12}|)s_{12} - \frac{V_2}{V_3}\kappa s_{23}^2 + \frac{V_2}{V_3}f_3 - f_2. \tag{29}$$

3.2. *Three stable regimes of flow*

Both overturning and estuarine circulations showed that stability of circulation regimes can be constrained by certain values of freshwater input (cf. Section 2), and we may expect similar constraints to apply to the three regimes of the double estuarine circulation. We now pose the question for what range of freshwater parameters f_2 and f_3 the three circulation regimes have stable solutions. To answer this question, we again solve for the equilibrium solutions in terms of salinity contrasts s_{12} and s_{23}, and determine the different bifurcations that limit the stability of the three regimes.

In eq. (27), we recognise the salt balance in basin 3 from Rooth's model [eq. (15)]. This reveals that we again have one equilibrium solution for s_{23},

$$s_{23}^* = \sqrt{\frac{f_3}{\kappa}}, \tag{30}$$

and consequently, the equilibrium transport of the estuarine branch, Ψ_E^*, is unaffected by the overturning branch [cf. eq. (19)]; it is still determined only by the freshwater input into basin 3. Hence, if there is no freshwater input into basin 3, there is no estuarine branch and the system is identical to Stommel's single overturning. This can be seen directly from eq. (28) with $f_3 = 0$ and $s_{23} = 0$.

With Stommel's solution for a single overturning appearing as the limiting solution for $f_3 = 0$, the question remains what solutions are possible with non-zero flow through the estuarine branch. The equilibrium solutions for s_{12} from eqns. (28) and (29) are:

$$s_{12}^* = \begin{cases} \frac{1}{2}(1+\sqrt{\kappa f_3}) \pm \sqrt{\frac{1}{4}(1+\sqrt{\kappa f_3})^2 - f_2} & \text{if } s_{12} \le 1, \\ \frac{1}{2} + \sqrt{\frac{1}{4}+f_2} & \text{if } s_{12} > 1+\kappa s_{23}, \\ \frac{f_2}{\sqrt{\kappa f_3}} & \text{if } 1 < s_{12} \le 1+\kappa s_{23}. \end{cases} \tag{31}$$

These three solutions apply to the *thermal, haline* and *throughflow* regimes, respectively (cf. Fig. 3a–c; with $f_3 = 0$ being the equilibria of Stommel, eq. (10).

The stable regions for the three circulation regimes, derived from eqns. (30) and (31), are shown in a phase-space diagram as a function of f_2 and f_3 (Fig. 4). Some of the limits of these stable regions are determined by saddle-node bifurcations (solid lines in Fig. 4). Each equilibrium solution in eq. (31) has one saddle-node bifurcation; for the thermal regime, this forms an upper limit for the freshwater input f_2 for which the circulation is stable; for the throughflow and haline regimes, it forms a lower limit. These saddle-node bifurcations can be expressed analytically as a function of f_3 (see also Appendix A):

$$f_2^{\mathrm{X}}|_{\mathrm{th}} = \frac{1}{4}(1+\sqrt{\kappa f_3})^2, \tag{32}$$

$$f_2^{\mathrm{X}}|_{\mathrm{ha}} = \kappa f_3 + \sqrt{\kappa f_3}, \tag{33}$$

$$f_2^{\mathrm{X}}|_{\mathrm{tf}} = \sqrt{\kappa f_3}. \tag{34}$$

Note that both equilibrium solutions and saddle-node bifurcations are independent on the basin volumes.

The only impact of basin volumes on the stability analysis of the double estuarine circulation comes from a Hopf bifurcation (dashed line in Fig. 4). This bifurcation

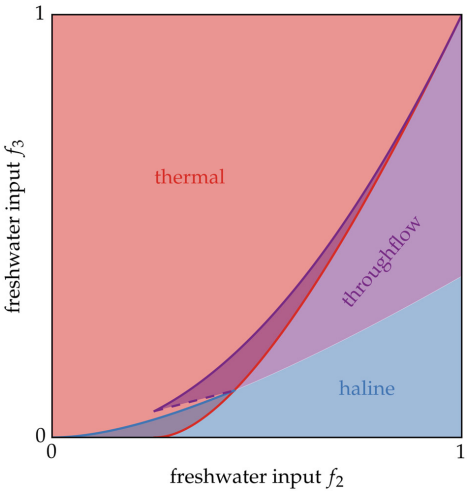

Fig. 4. Phase-space diagram for the double estuarine circulation. Colour shading indicates which circulation regime(s) can be stable as a function of both freshwater parameters f_2 and f_3. So-called bistability occurs where two regimes overlap. Solid lines indicate saddle-node bifurcations [cf. eqns. (32–34)]; the dashed line indicates a Hopf bifurcation [eq. (22)]. The diagram is drawn for the symmetrical case $\kappa = 1$ and $V_1 = V_2 = V_3$.

limits the stability of the throughflow regime by the same constraint as for the estuarine circulation [eq. (22)]. Crossing these bifurcations leads to an abrupt transition from one circulation regime to another. Continuous transitions between neighbouring regimes, however, are also possible. We observe that the throughflow and haline regimes do not share a common bistability region and as a result transitions between these two regimes are always continuous.

The (in)stability of the thermal circulation in the double estuary is governed by the same salt-advection feedback as was present in Stommel's two-box model. The point where this feedback deems the circulation unstable is determined by $f_2^{\mathrm{X}}|_{\mathrm{th}}$ [eq. (32)], which shifts to larger values of f_2 when f_3 increases (cf. red line in Fig. 4). For larger values of f_3, more freshwater is available to facilitate the estuarine branch. This branch provides additional salt from basin 1 into basin 2 and damps the salt-advection feedback. This delays a possible abrupt transition and allows for a thermal circulation to be sustained for larger values of freshwater input into basin 2 compared to the single overturning. The estuarine branch thus stabilises the thermal circulation.

4. Application to the Arctic Mediterranean

The Arctic Mediterranean – the Nordic Seas and Arctic Ocean combined – is perhaps the best known example of a large-scale double estuary. The exchanges across its main gateway, the GSR, are carried by three watermasses reflecting a double watermass transformation due to cooling and freshening. The initial transformation of Atlantic water induces buoyancy loss and production of dense water returning to the Atlantic as overflow water (Isachsen et al., 2007). The secondary transformation, occurring in the Arctic, is one of net buoyancy gain, producing low salinity water returning to the Atlantic as polar water (Rudels, 1989). The former loop is relatively dominant today, carrying about two-third of the circulation (cf. Table 1). The net water mass exchange at the GSR is thus associated with a relative dominance of heat loss and consequent buoyancy loss, and can therefore be characterised as a double estuarine circulation residing in its thermal regime. An illustration of thermal, haline and throughflow regimes in an Arctic Mediterranean setting is given in Fig. 3d–f.

Freshwater input into the Arctic Mediterranean is projected to increase over the 21st century (Rawlins et al., 2010), which makes this a region of interest with respect to changed surface buoyancy forcing. The qualitative analysis of our double estuary model in Section 3 revealed that an estuary branch can stabilise a thermally direct overturning. Using the Arctic Mediterranean as a specific example, we will illustrate the possible quantitative effect of this stabilisation.

We first interpret the model variables and parameters in the context of the Arctic Mediterranean and use observations to dimensionalise the model. We then place the present state of the circulation in the phase-space diagram (Fig. 4), and accordingly estimate the quantitative freshwater-sensitivity of a double estuarine circulation as illustrated by three hypothetical scenarios for increased freshwater input.

4.1. *Interpretation of the model*

The three basins of the box-model (Fig. 1c) are interpreted as reservoirs of the associated watermasses, as discussed in Section 2.3. Basin 1 then represents the above-thermocline North Atlantic, constituting warm, saline water; basin 2 represents the dense waters in the Nordic Seas; and basin 3 represents the reservoir of light polar water in the above-halocline Arctic Ocean and East Greenland Current.

For the volume exchange in and out of the Arctic Mediterranean, we neglect any volume fluxes associated with the Pacific inflow through the Bering Strait and with precipitation and river runoff. Both can be parametrised as contributions to freshwater input. Consequently, the only inflow of volume into the double estuary is that of warm saline Atlantic water, which will be interpreted as Ψ_{I}. The fraction of dense water produced in the Nordic Seas and Barents Sea that returns to the Atlantic as overflow water will be interpreted as Ψ_{O}. The residual densified inflow entrains into the polar water in the Arctic Ocean and ultimately exits through the East Greenland Current and Canadian Arctic Archipelago. The combined volume transport of this buoyant return flow to the Atlantic will be interpreted as Ψ_{E}. In order to redraw Fig. 4 for the double estuary of the Arctic Mediterranean, we need to estimate the relative basin volumes as well as κ.

The relative basin volumes determine the location of the Hopf bifurcation, limiting stability of the throughflow regime [eq. (22)]. Because the Arctic Mediterranean is a regional setting, we take $V_1 \gg V_{2,3}$, where the evaporating basin is arbitrarily large with respect to the Arctic Mediterranean. As discussed in Section 2.3, this limit makes the salinity of the Atlantic inflow independent on the freshwater input into the Arctic Mediterranean. Because Arctic polar water is confined by the halocline, whereas dense waters in the Nordic Seas extend to full depth through deep convection, we further take $V_2 \gg V_3$. In these limits, $f_3^{\mathrm{O}} = 0$, indicating that the throughflow regime is unrestricted by the Hopf bifurcation.

Parameter κ determines the locations of the saddle-node bifurcations [eqns. (32–34)]. Inserting observed density contrasts and volume transports (Tab. 1; Hansen and Østerhus, 2000; Eldevik and Nilsen, 2013) into eqns. (3) and (16), we find $\kappa = 0.32$. The scaling of the estuarine transport to density differences is thus a factor three smaller

than that of the overturning transport. If these transports are related to the hydrostatic pressure difference across isopycnals dividing the associated watermasses, k_O should scale with the depth of the thermocline above the GSR (about 600 m), and k_E should scale with the depth of the Arctic halocline (about 200 m). We see that this difference in isopycnal depth can largely account for the value of κ, deduced from observations.

4.2. *A relatively insensitive Atlantic inflow*

Scaling the complete system by these observations according to eqns. (4–6), we redraw the phase-space diagram for the double estuary of the Arctic Mediterranean (Fig. 5a). This diagram maps out the qualitative regions where the three circulation regimes have stable solutions. Using this diagram, we will determine the position of the 'present state' of the Arctic Mediterranean and quantify the required freshwater perturbation to induce an abrupt transition.

The present state of the double estuarine circulation is defined as the unique point in phase space where both Ψ_O^* and Ψ_E^* are equal to observed transports (cf. Fig. 5b). Equivalently, the present state in Stommel's model is defined where Ψ_O^* is equal to observed transport and Ψ_E^* is zero. The latter is naturally aligned with zero polar freshwater input.

Starting with the present state forcing (cf. Fig. 5c), we assess the following hypothetical scenarios for increased freshwater input into the double estuary:

A: only Nordic freshwater input increases.
B: all freshwater input increases proportionally.
C: only polar freshwater input increases.

Each of these scenarios is projected as dashed lines in Fig. 5c. Along each line, we determine the value of Ψ_I^* as a function of the varying freshwater input and draw a bifurcation diagram for the Atlantic inflow (Fig. 6).

In *Scenario A* (Fig. 6a), the increase in freshwater input always weakens the Atlantic inflow since all additional freshwater enters in the stage of buoyancy loss, limiting the transport of the overturning branch while leaving the estuarine branch constant. An increase in Nordic freshwater input of 37 mSv destabilises the thermal circulation and induces an abrupt transition to the haline regime (see also Fig. 5c). Neglecting the estuarine branch and collapsing the system to a single overturning circulation (Stommel's model), an increase in Nordic freshwater input of 14 mSv is sufficient to induce a transition to the haline regime. In the double estuary model, the estuary branch advects additional salt to the regions of dense water formation, delaying a possible abrupt transition.

In *Scenario B* (Fig. 6b), increased freshwater input partly weakens the overturning branch and partly strengthens the estuarine branch. Because the weakening of the overturning appears dominant in this scenario, an increase in the total freshwater input inhibits the net Atlantic inflow and can destabilise the thermal circulation. Compared to *Scenario A*, this requires a larger increase in the total freshwater input (123 mSv) because of the stabilising salt advection through the estuarine branch. If an abrupt transition occurs under *Scenario B*, the circulation transits into the throughflow regime (see also Fig. 5c). During such a transition a warm Atlantic inflow persists and the surface conditions of the Arctic Mediterranean remain qualitatively the same (compare Fig. 3d and f).

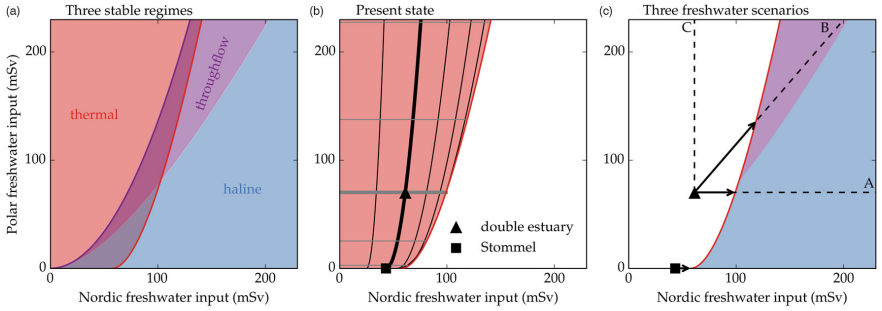

Fig. 5. Phase-space diagram for the Arctic Mediterranean. (a) As in Fig. 4, scaled as described in Section 4. (b) Stable region of the thermal regime. Contours, interval 1 Sv, indicate constant overturning (black) and estuarine transport (grey). Thick lines correspond to observed transports (cf. Table 1). Markers indicate the 'present state' in the double estuary model and in Stommel's model. (c) From the 'present state', three dashed lines indicate scenarios for increased freshwater input in the double estuary model. Arrows indicate the required freshwater increase along each scenario to induce an abrupt transition into either the throughflow or haline regime. An additional scenario is indicated for Stommel's model for increased Nordic freshwater input.

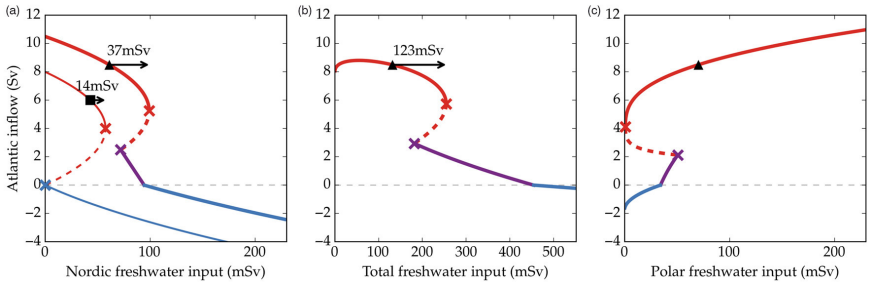

Fig. 6. Bifurcation diagram for three scenarios of increased freshwater input into the Arctic Mediterranean. Equilibrium solutions for Ψ_1^* are shown along the trajectories A, B and C indicated in Fig. 5c. As a reference, the bifurcation diagram of the overturning (Stommel, Fig. 2a) is shown in the left panel. 'Present state' (triangle and square) is defined in Fig. 5b. Arrows are equivalent to those in Fig. 5b, indicating the required freshwater increase to destabilise the thermal circulation and induce an abrupt transition. The three Scenarios A, B and C are described in detail in the text.

Finally in *Scenario C* (Fig. 6c), increased polar freshwater input merely strengthens the estuarine branch. The associated salt transport from the Atlantic even facilitates dense water formation and increases the transport of the overturning branch slightly (not shown). Together, this leads to a strengthening of the Atlantic inflow and no abrupt transitions can occur.

Scenario *B* illustrates a possible transition from a thermal to a throughflow regime (cf. Fig. 3d and f). In the latter regime, the Atlantic inflow which carries salt towards the Arctic Mediterranean to balance net freshwater input is both along the surface and at depth. A necessary condition for this circulation to be realisable is that this inflow originates from warmer waters. Although this is likely because of its origin in lower latitudes, the quantitative temperature contrast beyond a transition to the throughflow regime cannot be estimated from this model. Rather, it needs to be determined a priori and for the illustration of Fig. 6, the temperature contrast is kept equal for all circulation regimes.

With these three scenarios, we illustrate a wide variety of possibilities for how freshwater input can affect THC. The most important factor in determining the circulation's response is the distribution of additional freshwater input. Estimates of projected increase in freshwater input in the Arctic Mediterranean primarily point to the increase in river runoff into the Arctic Ocean (Rawlins et al., 2010). We may therefore imagine a scenario between *B* and *C* as most appropriate for discussing quantitative change of the Arctic Mediterranean's THC.

In between these scenarios, Atlantic inflow is relatively insensitive to increased freshwater input. Estimates of long-term trends in Arctic sea ice melt are on the order of 10 mSv (500 km^3/yr; Laxon et al., 2013). Whereas Stommel's model is very sensitive to a freshwater perturbation of this magnitude, it only impacts the double estuarine circulation significantly if all additional freshwater were to reach the Nordic Seas (cf. Fig. 6a). Rather than a significant change in the Atlantic inflow, the double estuary model shows a shift towards a more estuarine-dominated circulation where increased freshwater input weakens the overturning branch and strengthens the estuarine branch. A predominant role for freshwater in the branching of the circulation, rather than in restricting its total strength – the inflow – is also inferred from the diagnostics of Eldevik and Nilsen (2013).

5. Concluding remarks

GCMs used to quantify freshwater-induced changes in Atlantic THC in the framework of Stommel's box-model appear very sensitive to changes in northern freshwater input. Rahmstorf (1996) predicted a shutdown of the circulation when northern freshwater input is increased by 70 mSv. This value is comparable to the estimated increase in freshwater input into the Arctic and sub-Arctic seas over the 21st century, based on observations and model experiments (Rawlins et al., 2010).

Coupled atmosphere–ocean GCMs, projecting CO_2-induced changes in climate over this same period, however do not show a consistent sensitivity of the Atlantic THC to freshwater as opposed to heat (Gregory et al., 2005; Weaver et al., 2012). Specifically the northernmost branch of the THC in the Arctic Mediterranean appears less sensitive to freshwater than heat (Eldevik and Nilsen, 2013). By adding freshwater input in the order of 1.0 Sv into the North Atlantic in coupled GCMs, Stouffer et al. (2006) showed that deliberate water-hosing experiments are required to completely shut down the Atlantic overturning circulation. Our extension of Stommel's model into a double estuary illustrates how THC can be inherently more stable than a single overturning circulation.

The freshwater-sensitivity of a double estuarine circulation is qualitatively associated with the northern distribution of freshwater input. This distribution largely determines how additional total freshwater input may affect THC. In a limiting, most sensitive case where all freshwater feeds into the domain of dense water formation, the model is identical to that of Stommel (1961, Fig. 1a). The distribution of freshwater is directly linked to the pathways out of the double estuary, for example, in the case of the Arctic Mediterranean where much freshwater is exported via the East Greenland Current. Representation of the different watermass transformations and advective pathways additional to that of a single overturning circulation therefore appears essential for the freshwater-sensitivity of THC.

Our model for a double estuary accounts for a circulation branch that is sustained by buoyancy gain due to northern freshwater input: an estuarine branch, much like the Arctic estuarine circulation (Stigebrandt, 1981). This additional circulation branch damps Stommel's positive salt-advection feedback by providing a background salt import into the domain of dense water formation and hereby stabilises the overturning branch. A similar stabilisation was found when adding diffusion to Stommel's model to parametrise a wind-driven gyre (Longworth et al., 2005), and also Guan and Huang (2008); Nilsson and Walin (2001) concluded that THC is less sensitive to freshwater perturbations than Stommel's model when accounting for limited diapycnal mixing. These studies, including our study of a double estuary, all point in the same direction of a relatively weak freshwater-sensitivity of THC compared to that inferred from Stommel's model.

In the double estuary model, a proportional increase in northern freshwater input of 123 mSv is required to destabilise the overturning when an estuarine branch is accounted for (Fig. 6b). This value is an order of magnitude larger than the additional freshwater input required to destabilise the single overturning circulation of Stommel's model when scaled to the Arctic Mediterranean (Fig. 6a). Overall, a larger amount of freshwater feeding the estuarine branch allows the circulation to retain its qualitative state under larger increase in freshwater into the domain of dense water formation. For a certain range of distributions, additional northern freshwater input can even strengthen the THC (Fig. 6c). Because the overturning branch of the Arctic Mediterranean, including entrainment of Atlantic water into the overflows south of the GSR, is estimated to account for approximately 2/3 of the total AMOC (Dickson and Brown, 1994; Medhaug et al., 2012), stability of this northernmost branch of the Atlantic THC is important for sustaining a stable global overturning circulation (e.g. Jungclaus et al., 2006).

Abrupt reduction in THC is commonly associated with a cessation in open ocean convection (e.g. Dokken and Jansen, 1999). However, it is now understood that poleward heat transport and consequent northern heat loss are more directly related to ocean advection than convective mixing (Mauritzen, 1996; Fanning and Weaver, 1997; Pickart and Spall, 2007). Our model for the double estuary accommodates a third stable circulation regime, complementing the thermal and haline regimes introduced by Stommel. In this *throughflow* regime, the estuarine circulation dominates to the extent that net Atlantic inflow persists even in the case of absent or reversed overflow. This implies, at least in our model, that inflow can be sustained without dense water formation. More generally, we propose that an estuarine circulation extends the stability of poleward heat transport with respect to freshwater perturbations beyond the thermal regime.

6. Acknowledgements

This research was supported by the Centre for Climate Dynamics at the Bjerknes Centre for Climate Research through the Research Council of Norway project NORTH. Publication was funded by the University of Bergen. We thank Aleksi Nummelin, Lisbeth Håvik and two anonymous reviewers for their valuable input that improved the manuscript.

7. Appendix

A. Linear stability analysis

In order to determine whether a circulation can reside in a certain equilibrium state, we perform linear stability analysis on each equilibrium solution. This theory is based on linearisation of the model equations around a certain equilibrium and determining the growth rate of a perturbation. If this growth rate is negative, perturbations are damped and the equilibrium solution is stable; if the growth rate is positive, perturbations are amplified and the equilibrium is unstable.

Linearisation around an equilibrium is done by determining the Jacobian J. If the model consists of a single dynamical equation [as Stommel's model, cf. eq. (8)], this Jacobian is defined as:

$$J = \frac{\partial}{\partial s_{12}} \frac{ds_{12}}{d\tau}\bigg|_{s_{12}^*}, \tag{A1}$$

and the equilibrium s_{12}^* is stable if $J < 0$. At the boundary between a stable and an unstable equilibrium, where $J = 0$, a saddle-node bifurcation exists.

If the model consists of a system of two dynamical equations [as is the case for Rooth's model and our double estuary model, cf. eqns. (17), (18), (28) and (29)], the Jacobian is defined as:

$$J = \left(\begin{array}{cc} \frac{\partial}{\partial s_{12}} \frac{ds_{12}}{d\tau} & \frac{\partial}{\partial s_{23}} \frac{ds_{12}}{d\tau} \\ \frac{\partial}{\partial s_{12}} \frac{ds_{23}}{d\tau} & \frac{\partial}{\partial s_{23}} \frac{ds_{23}}{d\tau} \end{array} \right) \Bigg|_{s_{12}^*, s_{23}^*}. \tag{A2}$$

In this case, two conditions determine a stable solution: $det(J) > 0$ and $trace(J) < 0$. The boundary $det(J) = 0$ determines the location of a saddle-node bifurcation; $trace(J) = 0$ determines the location of a Hopf bifurcation. Since we are merely interested in the stability of an equilibrium, we do not distinguish between stable nodes and foci.

A.1. Overturning circulation (Section 2.1)

Inserting eq. (8) into eq. (A1), we find for Stommel's overturning circulation:

$$J = \begin{cases} -(1 + \frac{V_2}{V_1})(1 - 2s_{12}^*) & \text{if } s_{12} \le 1, \\ +(1 + \frac{V_2}{V_1})(1 - 2s_{12}^*) & \text{if } s_{12} > 1. \end{cases} \tag{A3}$$

As shown by Stommel (1961), for the thermal overturning ($s_{12} \le 1$), the negative root of eq. (10) is always stable and the positive root is unstable. The haline overturning ($s_{12} > 1$) is always stable. The points where stable and unstable equilibria meet are characterised by saddle-node bifurcations [eqns. (11) and (12)] as indicated in Fig. 2a.

A.2. Estuarine circulation (Section 2.2)

Inserting eqns. (17) and (18) into eq. (A2), we find for Rooth's estuarine circulation:

$$J = \begin{pmatrix} -(1 + \frac{V_2}{V_1})\sqrt{\kappa f_3} & -(1 + \frac{V_2}{V_1}) \frac{\kappa f_2}{\sqrt{\kappa f_3}} - 2\frac{V_2}{V_1}\sqrt{\kappa f_3} \\ \sqrt{\kappa f_3} & \frac{\kappa f_2}{\sqrt{\kappa f_3}} - 2\frac{V_2}{V_3}\sqrt{\kappa f_3} \end{pmatrix}, \tag{A4}$$

with

$$det(J) = 2\left(\frac{V_2}{V_3} + \frac{V_2^2}{V_1 V_3} + \frac{V_2}{V_1}\right)\kappa f_3, \tag{A5}$$

$$trace(J) = \frac{\kappa f_2}{\sqrt{\kappa f_3}} - \left(1 + \frac{V_2}{V_1} + 2\frac{V_2}{V_3}\right)\sqrt{\kappa f_3}). \tag{A6}$$

Since $det(J) > 0$ for all $f_3 > 0$, no saddle-node bifurcations limit the stability of the estuarine circulation. However, a Hopf bifurcation appears at $trace(J) = 0$, introducing a stability condition (cf. Scott et al., 1999),

$$f_3 > \frac{f_2}{1 + V_2/V_1 + 2V_2/V_3}, \tag{A7}$$

which divides between a stable and an unstable equilibrium [eq. (22)] as indicated in Fig. 2b.

A.3. Double estuarine circulation (Section 3)

For the double estuary model, it is most convenient to perform linear stability analysis on each circulation regime separately.

A.3.1. Thermal regime ($s_{12} \le 1$)

For the thermal regime, the Jacobian is:

$$J = \begin{pmatrix} -(1 + \frac{V_2}{V_1})(1 + \sqrt{\kappa f_3} - 2s_{12}^*) & -(1 + \frac{V_2}{V_1})\kappa s_{12}^* - 2\frac{V_2}{V_1}\sqrt{\kappa f_3} \\ (1 + \sqrt{\kappa f_3} - 2s_{12}^*) & \kappa s_{12}^* - 2\frac{V_2}{V_3}\sqrt{\kappa f_3}, \end{pmatrix} \tag{A8}$$

with

$$det(J) = 2\frac{V_2}{V_1}(1 + \sqrt{\kappa f_3} - 2s_{12}^*)(2 + \frac{V_2}{V_1})\sqrt{\kappa f_3}, \tag{A9}$$

$$trace(J) = -(1 + \frac{V_2}{V_1})(1 + \sqrt{\kappa f_3} - 2s_{12}^*) - 2\frac{V_2}{V_3}\sqrt{\kappa f_3} + \kappa s_{12}^*. \tag{A10}$$

As for the single overturning, a saddle-node bifurcation ($det(J) = 0$) appears, deeming the negative root of eq. (31) stable and the positive root unstable. This saddle-node bifurcation is expressed in terms of f_2 in eq. (11).

A Hopf bifurcation appears if $trace(J) = 0$ and $det(J) > 0$. This is possible if

$$\frac{V_2}{V_3} < \frac{1}{4} \frac{\kappa(1 + \sqrt{\kappa f_3})}{\sqrt{\kappa f_3}}. \tag{A11}$$

If f_2 increases, this Hopf bifurcation destabilises the thermal regime before the saddle-node bifurcation can be reached.

In the symmetrical case of $\kappa = 1$ and $V_1 = V_2 = V_3$ (cf. Fig. 4), a Hopf bifurcation appears if $f_3 < \frac{1}{9}$. It can be shown that the maximum distance from the saddle-node bifurcation $f_2^{\mathrm{X}}|_{\mathrm{th}}$ is 0.01 (in the case of $f_3 = 0$). This means that the thermal regime becomes unstable at $f_2 = 0.24$, rather than 0.25 as deduced from the saddle-node bifurcation. This effect is marginal, and no Hopf bifurcation can appear in the case of the Arctic Mediterranean where we take $V_2 \gg V_3$. We therefore do not pursue this possible instability further.

A.3.2. Haline regime ($s_{12} > 1 + \kappa s_{23}$)

For the haline regime, the Jacobian is:

$$J = \begin{pmatrix} (1 + \frac{V_2}{V_1})(1 - 2s_{12}^*) & -2\frac{V_2}{V_1}\sqrt{\kappa f_3} \\ -(1 - 2s_{12}^*) & -2\frac{V_2}{V_3}\sqrt{\kappa f_3}, \end{pmatrix} \tag{A12}$$

with

$$det(J) = -2\left(\frac{V_2}{V_1} + \frac{V_2^2}{V_1 V_3} + \frac{V_2}{V_3}\right)\sqrt{\kappa f_3}\,(1 - 2s_{12}^*), \qquad \text{(A13)}$$

$$trace(J) = \left(1 + \frac{V_2}{V_1}\right)(1 - 2s_{12}^*) - 2\frac{V_2}{V_3}\sqrt{\kappa f_3}. \qquad \text{(A14)}$$

Inserting eq. (31), we find that $det(J) > 0$, $trace(J) < 0$ for all values of f_2, $f_3 > 0$ and consequently the haline equilibrium always stable.

At the boundary between the haline and throughflow regimes, at $s_{12} = 1 + \kappa s_{23}$, a saddle-node bifurcation appears if the throughflow equilibrium is unstable, as expressed in eq. (29). If the throughflow equilibrium is stable, there is no saddle-node bifurcation for the haline regime and transitions between the haline and throughflow regimes are smooth.

A.3.3. Throughflow regime ($1 < s_{12} \le 1 + \kappa s_{23}$)

For the throughflow regime, the Jacobian is:

$$J = \begin{pmatrix} -\left(1 + \frac{V_2}{V_1}\right)\sqrt{\kappa f_3} & -\left(1 + \frac{V_2}{V_1}\right)\kappa s_{12}^* - 2\frac{V_2}{V_1}\sqrt{\kappa f_3} \\ \sqrt{\kappa f_3} & \kappa s_{12}^* - 2\frac{V_2}{V_3}\sqrt{\kappa f_3}, \end{pmatrix} \qquad \text{(A15)}$$

with

$$det(J) = 2\left(\frac{V_2}{V_1} + \frac{V_2^2}{V_1 V_3} + \frac{V_2}{V_3}\right)\sqrt{\kappa f_3}, \qquad \text{(A16)}$$

$$trace(J) = \kappa s_{12}^* - \left(1 + \frac{V_2}{V_1} + 2\frac{V_2}{V_3}\right)\sqrt{\kappa f_3}. \qquad \text{(A17)}$$

$det(J)$ always positive, so a saddle-node bifurcation occurs where the throughflow regime meets the unstable branch of the thermal equilibrium at $s_{12} = 1$, as expressed in eq. (34).

Because the dynamics and consequently the equilibrium solutions of the throughflow regime are identical to those of the estuarine circulation of Rooth, a Hopf bifurcation appears at the same point: $trace(J) = 0$ if $f_3 = \frac{f_2}{1 + V_2/V_1 + 2V_2/V_3}$, dividing a stable and an unstable throughflow circulation.

B. Salt conservation

Salt conservation in the double estuary model is expressed in single equations for each basin, general for each circulation regime [eqns. (25–27)]. Here, we provide the equations applied to each separate regime, dependent on the transport signs as indicated in Fig. 3a–c.

B.1. Thermal regime ($\Psi_I > 0$, $\Psi_O > 0$)

$$V_1\frac{dS_1}{dt} = -\Psi_I \Delta S_{12} - \Psi_E \Delta S_{23} + F_2 + F_3, \qquad \text{(B1)}$$

$$V_2\frac{dS_2}{dt} = \Psi_I \Delta S_{12} - F_2, \qquad \text{(B2)}$$

$$V_3\frac{dS_3}{dt} = \Psi_E \Delta S_{23} - F_3. \qquad \text{(B3)}$$

B.2. Haline regime ($\Psi_I < 0$, $\Psi_O < 0$)

$$V_1\frac{dS_1}{dt} = \Psi_O \Delta S_{12} - \Psi_E \Delta S_{23} + F_2 + F_3, \qquad \text{(B4)}$$

$$V_2\frac{dS_2}{dt} = -\Psi_O \Delta S_{12} - F_2, \qquad \text{(B5)}$$

$$V_3\frac{dS_3}{dt} = \Psi_E \Delta S_{23} - F_3. \qquad \text{(B6)}$$

B.3. Throughflow regime ($\Psi_I > 0$, $\Psi_O < 0$)

$$V_1\frac{dS_1}{dt} = -\Psi_E \Delta S_{12} - \Psi_E \Delta S_{23} + F_2 + F_3, \qquad \text{(B7)}$$

$$V_2\frac{dS_2}{dt} = \Psi_E \Delta S_{12} - F_2, \qquad \text{(B8)}$$

$$V_3\frac{dS_3}{dt} = \Psi_E \Delta S_{23} - F_3. \qquad \text{(B9)}$$

References

Bryan, F. 1986. High-latitude salinity effects and interhemispheric thermohaline circulations. *Nature*. **323**, 301–304.

de Boer, A. M., Gnanadesikan, A., Edwards, N. R. and Watson, A. J. 2010. Meridional density gradients do not control the Atlantic overturning circulation. *J. Phys. Oceanogr.* **40**(2), 368–380.

Dickson, R. R. and Brown, J. 1994. The production of North Atlantic Deep Water: sources, rates, and pathways. *J. Geophys. Res.* **99**(C6), 12319–12341.

Dokken, T. M. and Jansen, E. 1999. Rapid changes in the mechanism of ocean convection during the last glacial period. *Nature*. **401**(6752), 458–461.

Eldevik, T. and Nilsen, J. E. Ø. 2013. The Arctic–Atlantic thermohaline circulation. *J. Clim.* **26**(21), 8698–8705.

Fanning, A. F. and Weaver, A. J. 1997. A horizontal resolution and parameter sensitivity study of heat transport in an idealized coupled climate model. *J. Clim.* **10**(10), 2469–2478.

Gregory, J. M., Dixon, K. W., Stouffer, R. J., Weaver, A. J., Driesschaert, E. and co-authors. 2005. A model intercomparison of changes in the Atlantic thermohaline circulation in response to increasing atmospheric CO2 concentration. *Geophys. Res. Lett.* **32**(12), L12703.

Griesel, A. and Maqueda, M. A. M. 2006. The relation of meridional pressure gradients to north Atlantic deep water volume transport in an ocean general circulation model. *Clim. Dynam.* **26**(7–8), 781–799.

Guan, Y. P. and Huang, R. X. 2008. Stommel's box model of thermohaline circulation revisited—the role of mechanical energy supporting mixing and the wind-driven gyration. *J. Phys. Oceanogr.* **38**(4), 909–917.

Hansen, B. and Østerhus, S. 2000. North Atlantic-Nordic seas exchanges. *Prog. Oceanogr.* **45**(2), 109–208.

Isachsen, P. E., Mauritzen, C. and Svendsen, H. 2007. Dense water formation in the Nordic seas diagnosed from sea surface buoyancy fluxes. *Deep Sea Res. Part I Oceanogr. Res. Pap.* **54**(1), 22–41.

Jungclaus, J. H., Haak, H., Esch, M., Roeckner, E. and Marotzke, J. 2006. Will Greenland melting halt the thermohaline circulation? *Geophys. Res. Lett.* **33**(17), 1–5.

Knudsen, M. 1900. Ein hydrographischer lehrsatz. *Ann. Hydrogr. Marit. Meteorol.* **28**(7), 316–320.

Kuhlbrodt, T., Griesel, A., Montoya, M., Levermann, A., Hofmann, M. and co-authors. 2007. On the driving processes of the Atlantic meridional overturning circulation. *Rev. Geophys.* **45**(2004), 1–32.

Kuznetsov, Y. A. 2013. *Elements of Applied Bifurcation Theory*, Vol. 112. Springer Science & Business Media, New York.

Laxon, S. W., Giles, K. A., Ridout, A. L., Wingham, D. J., Willatt, R. and co-authors. 2013. Cryosat-2 estimates of arctic sea ice thickness and volume. *Geophys. Res. Lett.* **40**(4), 732–737.

Longworth, H., Marotzke, J. and Stocker, T. F. 2005. Ocean gyres and abrupt change in the thermohaline circulation: a conceptual analysis. *J. Clim.* **18**(13), 2403–2416.

Manabe, S. and Stouffer, R. 1988. Two stable equilibria of a coupled ocean-atmosphere model. *J. Clim.* **1**(9), 841–866.

Marotzke, J. 2000. Abrupt climate change and thermohaline circulation: mechanisms and predictability. *Proc. Natl. Acad. Sci. USA.* **97**(4), 1347–1350.

Mauritzen, C. 1996. Production of dense overflow waters feeding the North Atlantic across the Greenland-Scotland Ridge. Part 2: an inverse model. *Deep Sea Res. Part I Oceanogr. Res. Pap.* **43**(6), 807–835.

Medhaug, I., Langehaug, H. R., Eldevik, T., Furevik, T. and Bentsen, M. 2012. Mechanisms for decadal scale variability in a simulated Atlantic meridional overturning circulation. *Clim. Dyn.* **39**(1–2), 77–93.

Nilsson, J. and Walin, G. 2001. Freshwater forcing as a booster of thermohaline circulation. *Tellus A Dyn. Meteorol. Oceanogr.* **53**(5), 629–641.

Pickart, R. S. and Spall, M. A. 2007. Impact of Labrador Sea convection on the North Atlantic meridional overturning circulation. *J. Phys. Oceanogr.* **37**(9), 2207–2227.

Rahmstorf, S. 1996. On the freshwater forcing and transport of the Atlantic thermohaline circulation. *Clim. Dyn.* **12**(12), 799–811.

Rahmstorf, S., Crucifix, M., Ganopolski, A., Goosse, H., Kamenkovich, I. V. and co-authors. 2005. Thermohaline circulation hysteresis: a model intercomparison. *Geophys. Res. Lett.* **32**(23), L23605.

Rawlins, M. A., Steele, M., Holland, M. M., Adam, J. C., Cherry, J. E. and co-authors. 2010. Analysis of the Arctic system for freshwater cycle intensification: observations and expectations. *J. Clim.* **23**(21), 5715–5737.

Rooth, C. 1982. Hydrology and ocean circulation. *Prog. Oceanogr.* **11**(2), 131–149.

Rudels, B. 1989. The formation of Polar Surface Water, the ice export and the exchanges through the Fram Strait. *Prog. Oceanogr.* **22**, 205–248.

Rudels, B. 2010. Constraints on exchanges in the Arctic Mediterranean—do they exist and can they be of use? *Tellus A Dyn. Meteorol. Oceanogr.* **62**(2), 109–122.

Rudels, B. 2012. Arctic ocean circulation and variability – advection and external forcing encounter constraints and local processes. *Ocean. Sci.* **8**(2), 261–286.

Scott, J. R., Marotzke, J. and Stone, P. H. 1999. Stability of the interhemispheric thermohaline circulation in a coupled box-model. *J. Phys. Oceanogr.* **29**(2–4), 415–435.

Stigebrandt, A. 1981. A model for the thickness and salinity of the upper layer in the Arctic ocean and the relationship between the ice thickness and some external parameters. *J. Phys. Oceanogr.* **11**(10), 1407–1422.

Stigebrandt, A. 1985. On the hydrographic and ice conditions in the northern North Atlantic during different phases of a glaciation cycle. *Palaeogeogr. Palaeoclimatol. Palaeoecol.* **50**, 303–321.

Stommel, H. M. 1961. Thermohaline convection with two stable regimes of flow. *Tellus.* **13**(2), 224–230.

Stouffer, R. J., Yin, J., Gregory, J. M., Dixon, K. W., Spelman, M. J. and co-authors. 2006. Investigating the causes of the response of the thermohaline circulation to past and future climate changes. *J. Clim.* **19**(8), 1365–1387.

Thual, O. and Mcwilliams, J. C. 1992. The catastrophe structure of thermohaline convection in a two-dimensional fluid model and a comparison with low-order box-models. *Geophys. Astrophys. Fluid Dyn.* **64**, 67–95.

Toggweiler, J. and Samuels, B. 1995. Effect of drake passage on the global thermohaline circulation. *Deep Sea Res. Part I Oceanogr. Res. Pap.* **42**(4), 477–500.

Wåhlin, A. K. and Johnson, H. L. 2009. The salinity, heat, and buoyancy budgets of a coastal current in a marginal sea. *J. Phys. Oceanogr.* **39**(10), 2562–2580.

Weaver, A. J., Sedláček, J., Eby, M., Alexander, K., Crespin, E. and co-authors. 2012. Stability of the Atlantic meridional overturning circulation: a model intercomparison. *Geophys. Res. Lett.* **39**(20), L20709.

Welander, P. 1986. Thermohaline effects in the ocean circulation and related simple models. In: *Large-Scale Transport Processes in Oceans and Atmosphere* (eds. J. Willebrand and D. L. T. Anderson). Dordrecht, Springer, Netherlands, pp. 163–200.

Werenskiold, W. 1935. Coastal currents. *Geophys. Publ.* **10**(13), 1–14.